International Journal of Computational Intelligence Research.
ISSN 0973-1873 Vol.3, No.3 (2007), pp. 231-252

Aerodynamic Shape Optimisation of Unmanned Aerial Vehicles using Hierarchical Asynchronous Parallel Evolutionary Algorithms

D.S. Lee[1], L.F. Gonzalez[2], K.Srinivas[3], D.J. Auld[4] and K.C.Wong[5]

[1-5]*School of Aerospace Mechanical Mechatronic Engineering, University of Sydney, NSW 2006, Australia*
dongseop.lee@aeromech.usyd.edu.au, gonzalez@aeromech.usyd.edu.au, ragh*@aeromech.usyd.edu.au*
douga@aeromech.usyd.edu.au, kc@aeromech.usyd.edu.au

***Abstract*: One of the challenges in Unmanned (Combat) Aerial Vehicles (UCAV) is the improvement of aerodynamic performance to complete diverse missions, increase endurance and lower fuel consumption. Recent advances in design tools, materials, electronics and actuators have opened the door for implementation of transonic flow control technologies to improve aerodynamic efficiency. This paper explores the application of a robust Multi-Objective Evolutionary Algorithm (MOEA) for the design and optimisation of aerofoil sections and wing planform of UAVs and UCAVs. The methodology is based on a canonical evolution strategy and incorporates the concepts of hierarchical topology, parallel computing and asynchronous evaluation. For the design and optimisation of UCAV wing planform shape, an aero-diamond planform shape with a jagged trailing edge is considered like saw tooth. Results obtained from the combination between the approach and the aerodynamic analysis tools show the improvement of the aerodynamic efficiency, a set of shock-free aerofoils and the supercritical aero-diamond wing. Results also indicate that the method is capable to produce non-dominated solutions.**

***Keywords*:** Multi-objective Evolutionary Algorithms**,** UAVs (Unmanned Aerial Vehicles) Design and optimization**.**

NOMENCLATURE

AR	= aspect ratio
S	= wing wetted area
C_R	= root chord length
b	= span length
$\lambda_{R\text{-}B}$	= inboard taper ratio
$\lambda_{B\text{-}T}$	= outboard taper ratio
$\Lambda_{R\text{-}B}$	= inboard sweep angle
$\Lambda_{B\text{-}T}$	= outboard sweep angle
$BP_{Inboard}$	= inboard break point
$BP_{Outboard}$	= outboard break point
$\Gamma_{R\text{-}B}$	= inboard dihedral angle
$\Gamma_{B\text{-}T}$	= outboard dihedral angle
M_∞	= free stream Mach number
Re	= Reynolds number
α	= angle of attack
ψ	= yaw angle
C_L	= lift coefficient
C_D	= drag coefficient
C_{D0}	= drag coefficient at zero lift
L/D	= lift to drag ratio

I. Introduction

UCAVs are a subclass of the UAVs with the potential to reduce the risk to human life in combat operation, increase the redundancy requirements and improve the effectiveness and efficiency of the mission. The missions for an UAV/UCAV can be diversified in terms of air-air, air-ground or both. To complete the diverse mission, the improvement of aerodynamic performance is one of the essential factors. The improvement of the aerodynamic performance of UAV/UCAVs can be achieved by optimising the aerofoil shapes for the aerofoil sections[2, 5, 8, 17, 22] and wing planform[3, 12, 13, 25]. For the stealth function, the minimisation of the visual signature, infrared heat signature, acoustic signature, radio transmission signature and radar echo signature can provide a low observable aircraft[15, 21, 28, 31]. A traditional approach in design optimisation is the use of gradient-based techniques. The gradient-based techniques are effective when applied to specific problems and within a specified range. The traditional methods are able to find optimal global solutions if the objective and constraints are differentiable. However, the traditional approaches will have difficulty to find optimal global solutions if a broader application of the optimiser is desired:

- When the complexity of the problem arises.
- If the problem considers multi-modal.
- Involves approximations.
- When the objective and constraints are not

differentiable.
- Involves multiple objectives and physics.

In the practical aerospace design and optimisation problem, some of above conditions are often considered. Therefore robust and alternative numerical tools are required. A relatively novel technique Evolutionary Algorithms (EAs) search for multiple points in the design space instead of moving from a single point and require no derivatives or gradients of the objective function. EAs have the capability of finding globally optimum solutions, are easy to process in parallel and can be easily adapted to aerodynamic analysis codes without major modification.

In this paper, a methodology was developed for the aerodynamic optimisation of the wing aerofoil sections and planform using a MOEA. The technique is based on canonical evolution strategies[20,24] and incorporates the concepts of hierarchical topology, asynchronous evaluation and Pareto tournament.

The rest of paper is organised as follows; the description of the methodology is given in section •. The formulation of the optimisation problem is described in section •. The validation of aerodynamic analysis tools used in this research is described in Section •. Section • presents optimisation rationale and algorithms. The application of the method to real world problems are shown in section •. Finally, Section • contains conclusions and directions for future research.

II. Methodology

The method couples the Hierarchical Asynchronous Parallel Evolutionary Algorithms (HAPEA) with several aerodynamic analysis tools for the design and optimisation of UCAV aerofoil sections and planform shapes. The algorithm is based on canonical Evolution Strategies[22, 26] and incorporates with the concepts of Covariance Matrix Adaptation (CMA)[16-18], Distance Dependent Mutation (DDM), a hierarchical topology, asynchronous evaluation and a Pareto tournament selection. This approach is applicable to single or multi-objective problems.

A. Hierarchical Topology (Multi-fidelity)

The hierarchical topology (fidelity) can provide different models including precise, intermediate and approximate models. Each node in topology can be handled by a different EAs code. The concepts of the hierarchical approach; displaying the relationship between the given layers are shown in Figure 1. Of particular interest in the circulation of solutions stems from the fact that each node can be handled by different EA code, having specific parameters that can be tuned. The best solutions progress from the third layer to the first layer where they are refined. The characteristics of each layer are discussed below:

1. The first layer incorporates the most precise formulation of the solver to refine the solution. This is achieved through manipulation of the EA to make the mutation take very small steps, thus refining the resolution.

2. The second layer is a compromise between exploitation and exploration. This layer incorporates an intermediate approximation of the solver or medium resolution.

3. The third layer is devoted to exploration; allowing the EA to take a broad sample space in the search domain via a large mutation span. The solver in this layer is by far the crudest approximation of the group with the coarsest resolution.

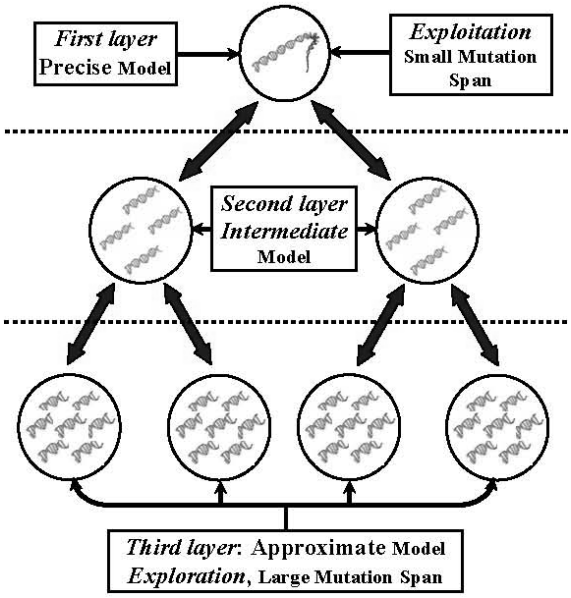

Figure 1: Hierarchical topology.

The inherent issue that arises in implementation of the hierarchical structure is time dependency. Where the first layer uses a very precise model to deliver a time-consuming solution, the sub-populations of the third layer use an approximate result to explore the search space; implying that good simple models can be used with fast solvers.

Further, all third layer nodes use a less accurate, faster model to compute the fitness function of the individuals of their populations. However roughly evaluated the solutions may be: the hierarchical topology presented earlier allows their information content to be used. This is permitted as the rigour of the second layer will scrutinize the quality of the solution through re-evaluation with a more precise model. Still, the intermediate model remains also a compromise, as it is deliberately not too precise for the sake of speed. And thus the process is repeated again by sending the solutions up to the top layer during the migration process. These solutions are re-evaluated to the most precise model that gives a genuinely accurate value for the fitness function.

B. Parallel Computing and Asynchronous Evaluation

EAs are particularly adaptable to parallel computing, especially when implemented using the master-slave approach[13]. Effectively, the master computer carries on the

optimisation process while the remote slave machines compute the solver code. The advantage being that the remote solvers do not need to run at the same speed or even on the same local network. Further, throughout the execution, solver nodes can be added or deleted at will. A schematic of such an implementation is shown in Fig. 2.

The distinctive method of an asynchronous approach is in generating only one candidate solution at a time and only re-incorporating one individual at a time. This differs with traditional EAs based on the canonical Evolution Strategy[13] that evaluates entire populations simultaneously. As a result, solutions can be generated and returned out of order. The method allows the implementation of an asynchronous fitness evaluation thus, giving the method its name. This is an extension of the work by Wakunda and Zell[18].

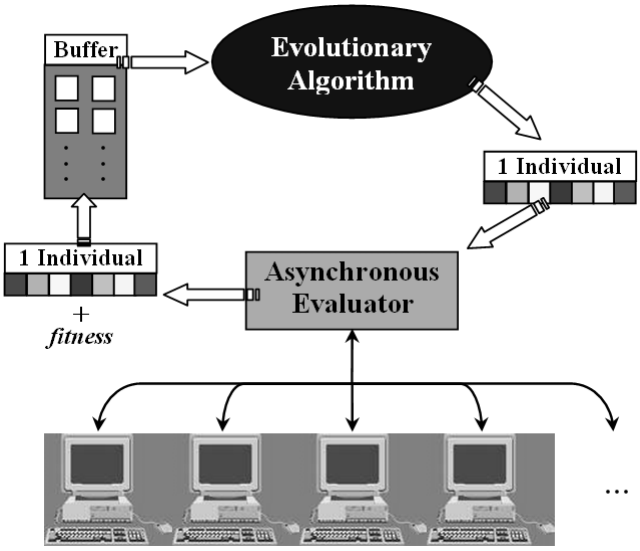

Figure 2. Parallel computing and asynchronous evaluation.

With an asynchronous approach there is no waiting time for individuals to return. As soon as a solution is available, it is incorporated back into the optimisation process. Credibility of the solution is checked via a separate evaluation buffer (*B*) that provides a statistical 'background check' on the comparative fitness of the solution. This buffer must have length comparative to the population size, but need not be too large; approximately twice the population size is more than sample. When an individual has had a fitness assigned, it is then compared to past individuals (both accepted and rejected) to determine whether or not it should be inserted into the main population. If it is to be accepted, then some replacement strategy is invoked and it replaces a member of the main population. Priority is given to the worst candidate always chosen from the population to be replaced that is called replace-worst-always method for the evaluation. The algorithm used in this research has been tested and parallelised using the Parallel Virtual Machine (PVM) framework[19]. Solid performances through several mathematical and real world test problems were evidenced.[20,21,22,23].

C. Multi-Criteria Optimisation

Design problems associated in the aeronautical discipline often require the simultaneous optimisation of conflicting objectives with associated number of constraints. Unlike single objective optimization problems, the solution is a set of points known as Pareto optimal set. Solutions are compared to other solutions using the concept of Pareto dominance. A multi-criteria optimisation problem can be mathematically formulated and consists of a number of objectives with a number of equality and inequality constraints as follows:

$$Maximise / Minimise \quad f_i(x) = 1, 2, ..., I$$

Subject to

$$g_j(x) = 0 \quad j = 1, 2, ..., J \quad \textit{equality constraints}$$

$$h_k(x) \le 0 \quad k = 1, 2, ..., K \quad \textit{inequality constraints}$$

Where f_i are the objective functions, I is the number of objectives, x is an n - dimensional vector containing n design or decision variables. For a minimisation problem, a vector x_1 is said less than vector x_2 if:

$$\forall_i f_i(x_1) < f_i(x_2) \text{ and } \exists_i f_i(x_1) < f_i(x_2)$$

In this case the solution $\boldsymbol{x_1}$ ***dominates*** the solution $\boldsymbol{x_2}$.

Most real world problems involve a number of inseparable objectives where there is no unique optimum, but a set of compromised individuals known as Pareto optimal (or non-dominated) solutions. The Pareto optimality principle is defined where a solution to a multi-objective problem has no other solutions that better satisfy all the objectives simultaneously.

The ability of EAs in evaluating multiple populations of points enables them of finding a number of solutions in a Pareto set. Pareto selection ranks the population and selects the non dominated individuals for the Pareto fronts. An EA that has capabilities for multi-objective optimisation is termed MOEAs. Theory and applications of MOEAs can be found in Reference [11-14]. A particular instance of MOEAs, are Hierarchical Asynchronous Parallel Evolution Algorithms (HAPEA).

D. Pareto Tournament Selection

The Pareto tournament selection was implemented by the authors through the "on-the-fly" selection operator. Through the on-the-fly selection operator, the self-calibrating EAs are able to adjust their parameters during the run as well as resizing the population (Ref:Evolutionary Algorithms With On-The-Fly Populationsize Adjustment). To implement an optimisation algorithm that is equally applicable to both single and multi-objective problems, a suitable selection

operator capable of handling either situation must be developed. The authors propose an extension of the standard tournament operator popular in many approaches [4,13,26]. The Pareto optimality approach[9] is used by the authors in this work.

Most MOEAs configured for multi-objective optimisation currently use the non-dominated sorting approach[36-38] that adapts an algorithm that is designed as a single objective optimiser into a multi-objective optimizer and is used by many researchers[7, 8, 13]. The problem with sorting approaches is that the method is not a fully integrated one. In practice, a sorting method works by computing the set of non-dominated solutions amongst a large statistical sampling (either a large population or previous data), and assigning these solutions as rank one.

Then ignoring these points, the process is repeated until a 'second' Pareto front is found, and this is assigned rank two. This process is reiterated until all points are ranked, and the value of the final rank is assigned to the individual as a new single objective fitness. The inherent problem arises then, on whether it is fair to assign individuals in the second rank numerically half the fitness of the first, and whether the third rank deserves a third of the fitness of the first.

The dilemma arises regarding the level of equality present amongst the solutions, as often solutions with excellent information may lie adjacent to, but not in: rank one. To solve this 'artificial scaling' problem, it is possible to introduce scaling, sharing and niching schemes[8], however all of these require problem-specific parameters or knowledge, even in adaptive approaches. The current operator requires no additional 'tuning' parameters and works seamlessly with the evaluation buffer (*B*) that explained in section II. B.

As illustrated in Fig. 3, the criteria for selection into the main population requires that the individual *x* be compared with the selection buffer (*B*) by assembling a small subset of this buffer called the tournament $Q = [q_1, q_2, ..., q_n]$ where Q is assembled by selecting individuals from the buffer (*B*), exclusively at random, until it is full. The process ensures that the new individual is not dominated by any other in the tournament and inserted into the population according to the replace-worst-always rules.

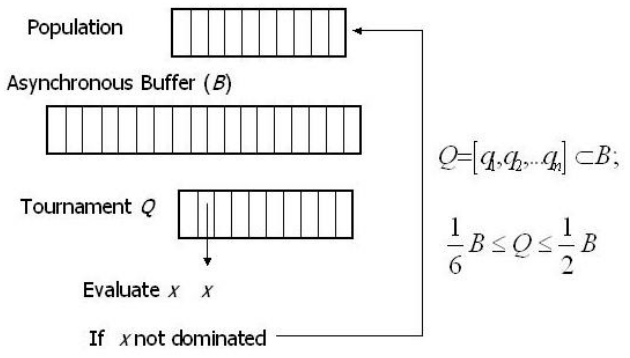

Figure 3. Pareto tournament selection operation.

The only parameter that needs to be determined in advance is the tournament size, a parameter that would exist as a single objective optimisation nonetheless. Selection of this parameter requires a small amount of problem specific knowledge, and should vary between $Q = B/2$ (strong selective pressure) and $Q = B/6$ (weak selective pressure). Although the optimizer is not overly sensitive to this value Q, in the absence of healthier information, the user is encouraged to opt for weak selective pressure (smaller tournaments). The democratic selection process of selecting individuals at random ensured good diversity amongst the selected individuals and no niching or forced separation of individuals was necessary. An example of it is illustrated in section III. A for the TNK mathematical problem. It can be seen that this methodology produced the correct Pareto front with a good diversity in the solutions. It can also be seen that in the event the fitness vectors have only one element (a single objective optimisation), this operator simplifies to the standard tournament selection operator[13, 17].

III. Validation of Methodology

Two simple test cases are considered to validate this approach: mathematical and inverse aerodynamic problems.

A. Mathematical (TNK) Problem

The TNK is an example of a constrained problem that has a discontinuous optimal Pareto front. This test consists of two objectives with two inequality constraints as follows:

TNK

$$f_1(x) = x_1$$
$$f_2(x) = x_2$$

Subject to constraints;

$$C_1(x) \equiv x_1^2 + x_2^2 - 1 - 0.1 \times \cos\left(16 \times \operatorname{atan}\left(\frac{x_1}{x_2}\right)\right) \geq 0$$
$$C_2(x) \equiv (x_1 - 0.5)^2 + (x_2 - 0.5)\, x_1^2 \leq 0.5$$

Design bounds;

$$0 \leq x_1 \leq \pi,\ 0 \leq x_2 \leq \pi$$

Two design variables are considered and population size of 100 is applied. This problem uses a discrete recombination approach to enable the capture of complex Pareto fronts. As illustrated in figure 4, it is shown that the algorithm has correctly distributed all individuals across the Pareto front for both test problems. Furthermore it is seen that even without any explicit niching or redistribution, individuals in the population are very evenly spread across the front.

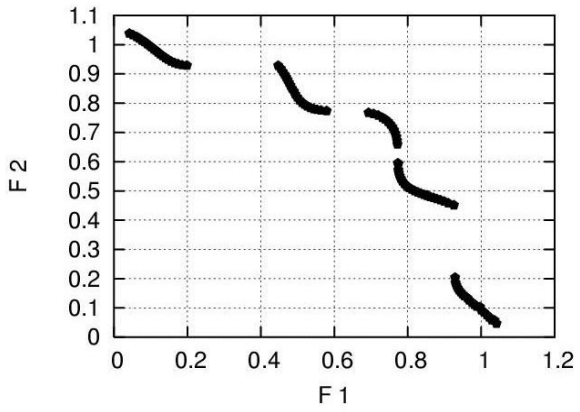

Figure 4: Pareto Front TNK.

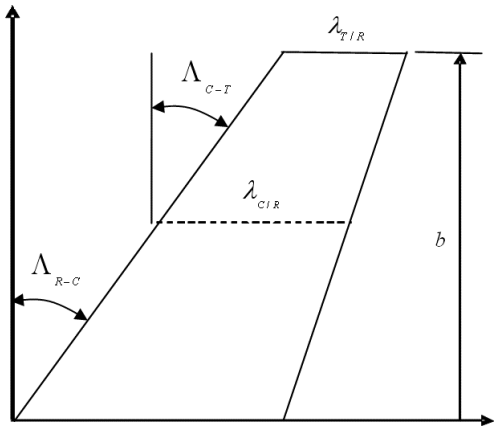

Figure 7. ONERA M6 wing geometry.

B. Inverse Aerodynamic Design Problem

1) Problem Definition

This test case considers the coupling and validation of the methodology for single-objective inverse aerodynamic design of ONERA M6 wing operating at transonic speeds. This problem has single-objective that consists of minimising of the difference between computed wing surface pressure distributions and pre-defined ONERA M6 wing pressure distributions. The flow conditions are illustrated in table 4. Fitness function is as follows;

$$f = \min\left(\frac{1}{n+m}\left[abs\left(\sum_{i=1}^{n}\left(\sum_{j=1}^{m}\left(Cp_{\text{Target}} - Cp_{\text{Candidates}}\right)\right)\right)\right]\right)$$

where i and j indicate chord-wise and span-wise number of wing sections.

Variables	M_∞	α	ψ	Re
Values	0.8395	3.06°	0°	11.72×10^6

Table 4. Flight conditions.

2) Design Variables

In this test considered, the external geometry of the wing planform is fixed as illustrated in Fig. 7 and table 5. The control points that define the aerofoil sections at three spanwise stations represent the design variables. The aerofoil geometry is represented using Bézier curves with the combination of a mean line and thickness distribution, which will be explained in section IV and V. A variable numbers of intermediate control points whose *x*-positions are fixed in advance and whose *y*-heights form the problem unknowns as illustrated in Fig. 8. The computed *Cp* will be compared to 21 spanwise sections [0:5:100] with 5% increment and 107 chordwise sections.

Variables	AR	b	Λ_{R-C}	Λ_{C-T}	$\lambda_{C/R}$	$\lambda_{T/R}$	$\Gamma_{Overall}$
Values	3.81	2.39 *ft*	30°	30°	0.781	0.562	0°

Table 5. ONERA M6 wing configurations.

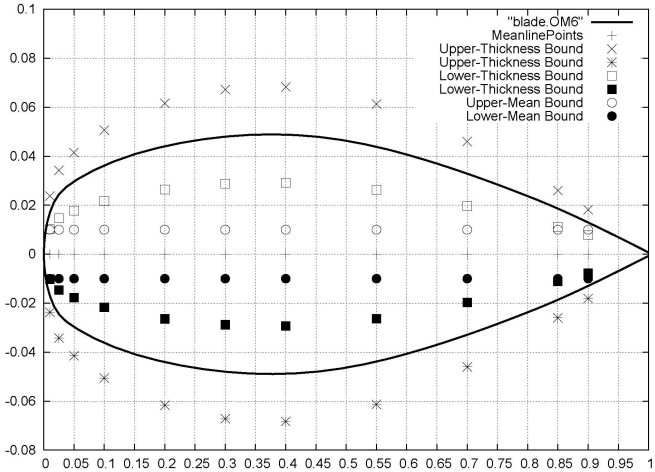

Figure 8. Aerofoil sections mean line and thickness control points design envelope.

3) Implementation

Potential flow solver FLO22 is utilised as an aerodynamic analysis tool and consider the following parameters for *Hierarchical Topology*.

First Layer: Population size of 20 with a computational grid of 96 × 12 × 16 cells.

Second Layer: Population size of 40 with a computational grid of 82 × 12 ×16 cells.

Third Layer: Population size of 60 with a computational grid of 68 × 12 × 16 cells.

4) Results

This problem was run for 450 function evaluations of the head node, and took approximately eighty hours. Figure 9 shows the optimisation progress history for this test case and

it is converged around 280 function evaluations. The geometries of optimised aerofoil sections are compared to target aerofoil (Baseline) in Fig. 10. As illustrated, there is a good match between aerofoils geometries Fig 11a also shows that there is a good match on the computed and target surface pressure distribution. Spanwise (0, 20, 40, 60, 80 and 90%) *Cp* distributions are illustrated in figures 5b to 5d and they are formed all most equal shapes of target *Cp* distributions.

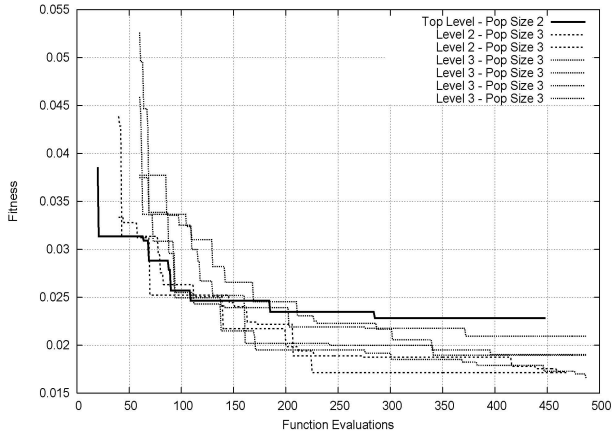

Figure 9. Optimisation progress history.

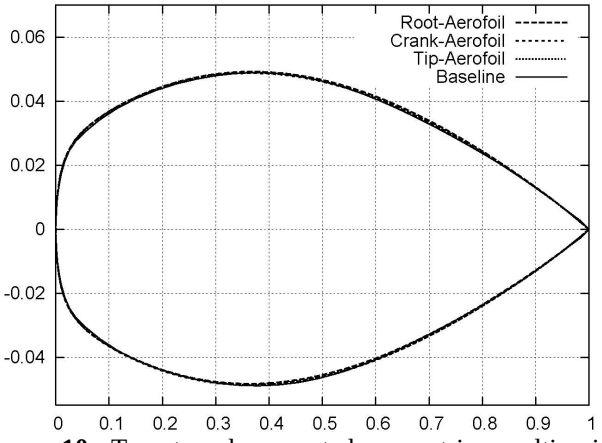

Figure 10. Target and computed geometries multi-point aerofoil design.

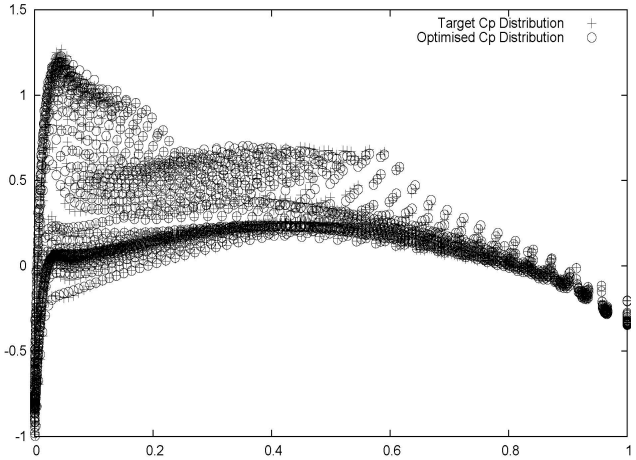

Figure 11a. Target and computed pressure distribution for multi-point aerofoil design.

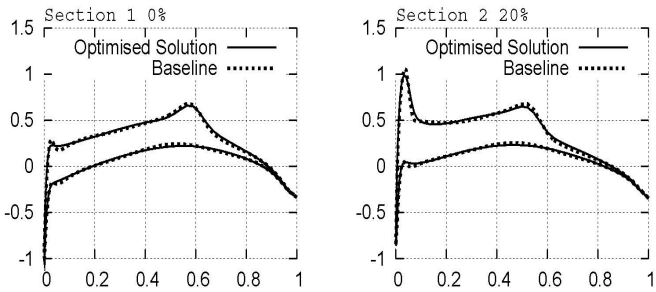

Figure 11b. Target and computed pressure distribution at 0 and 20% of span

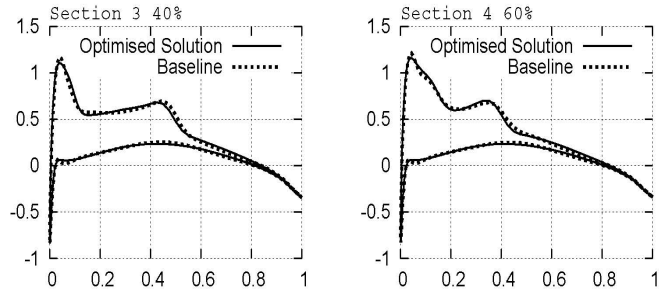

Figure 11c. Target and computed pressure distribution at 40 and 60% of span

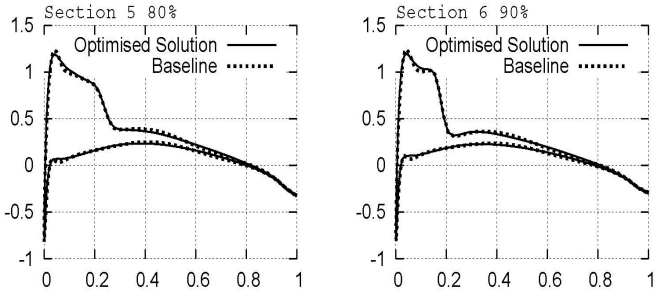

Figure 11d Target and computed pressure distribution at 80 and 90% of span

Concluding this case; the capabilities of this approach to find optimal shapes for inverse aerofoil sections shape optimisation problems is demonstrated. Without any problem specific knowledge, the method has captured the correct pressure distribution over different aerofoil sections operating at transonic speed.

IV. Aerodynamic Analysis Tools

There are several complexities involved when considering flow at transonic speeds. A proper selection and validation of analysis tools is required before coupling it with an optimisation process. A flow solver should meet some essential requirements such as: result accuracy, time consumption and robustness.

It is always desirable to use a high fidelity Navier-Stokes solver which accounts for the flow complexities at transonic speeds. The problem of using full Navier-Stokes solver is the computational expense of the solution as one computation on wing might take several hours on a supercomputer. In this

work, a low/middle fidelity potential flow solver is validated and introduced to reduce the computational expense.

A. Potential flow solver (FLO22)

The potential flow solver used in this research (FLO22)[20] is designed for analysing inviscid, isentropic, transonic flow past 3D swept wing configurations. The free stream Mach number is restricted only by the isentropic assumption and weak shock waves are automatically located wherever they occur in the flow. The finite-difference form of the full equation for the velocity potential is solved by the method of relaxation, after the flow exterior to the airfoil is mapped to the upper half plane. Further details on the solver can be found in the Reference 20. Fiction drag is externally computed by utilising program FRICTION.

B. Friction Drag (FRICTION)

The FRICTION program was developed by Hendrickson[25] and provides an estimate of laminar and turbulent the skin friction suitable for use in aircraft preliminary design.

Two test cases are considered to validate the aerodynamic analysis tools for optimisation.

1) Validation Test case I: ONERA M6 ($\alpha = 3.06°$)

This test case considers the ONERA M6 wing[35] operating at transonic speeds. The flow conditions are illustrated in table 1. For the computation the authors initially apply a computational grid with 96 cells in the chord-wise *x*-direction, 12 cells in the normal *y*-direction and 16 cells in the spanwise *z*-direction with 200 iterations. Then a fine grid with 192 cells in the chord-wise *x*-direction, 24 cells in the normal *y*-direction and 32 cells in the spanwise *z*-direction with 100 iterations.

Variables	M_∞	α	ψ	*Re*
Values	0.8395	3.06°	0°	11.72×10^6

Table 1. Flight conditions.

Results

The CPU time for this computation was 62.673s on a single 1.8GHz processor. The results from FLO22 and experimental data obtained by Schmitt and Charpin (1979)[35] at six spanwise sections (20%, 44%, 65%, 80%, 90% and 95%) are compared in Fig. 5 where lines represent FLO22 and dots for the wind tunnel data. There was a bit difference at 80%span *Cp* distribution. In overall, there is a good agreement between FLO22 and wind tunnel data.

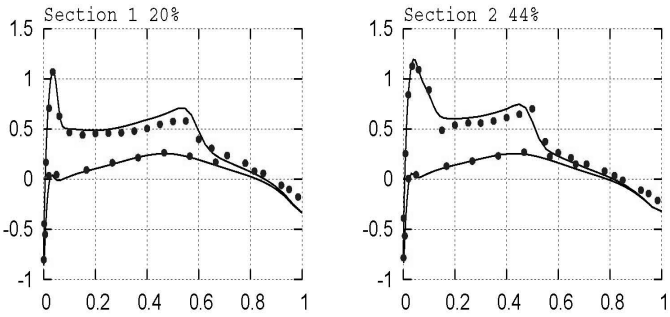

Figure 5a. C_P distribution at 20% and 44% of wing span.

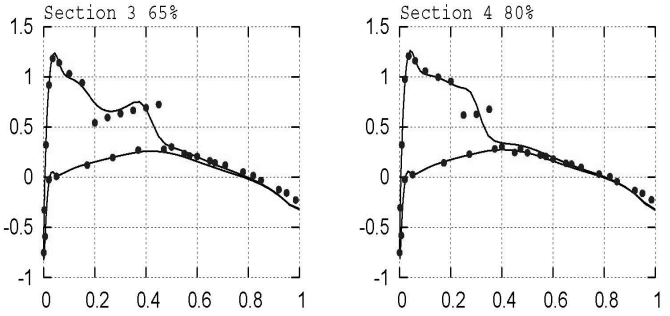

Figure 5b. C_P distribution at 65% and 80% of wing span.

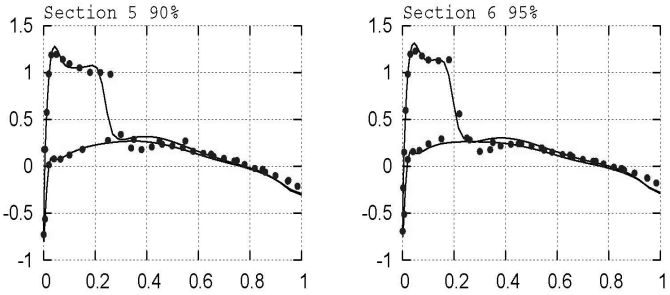

Figure 5c. C_P distribution at 90% and 95% of wing span.

2) Validation Test case II: ONERA M6 ($\alpha = 5.06°$)

This second test considers the ONERA M6 wing operating at the flow conditions indicated in table 2. The problem was solved using a computational grid of 96 × 12 × 16 for 200 iterations and then a 192 × 24 × 32 grid for 100 iterations.

Variables	M_∞	α	ψ	*Re*
Values	0.8395	5.06°	0°	11.72×10^6

Table 2. Flight conditions.

Results

The CPU time for this computation was 62.673s on a single 1.8GHz processor. Figure 6 compares the results obtained by FLO22 and experimental data obtained by Schmitt and Charpin (1979)[35] at six different spanwise sections (20%, 44%, 65%, 80%, 90% and 95%). A good agreement is settled between FLO22 and wind tunnel data.

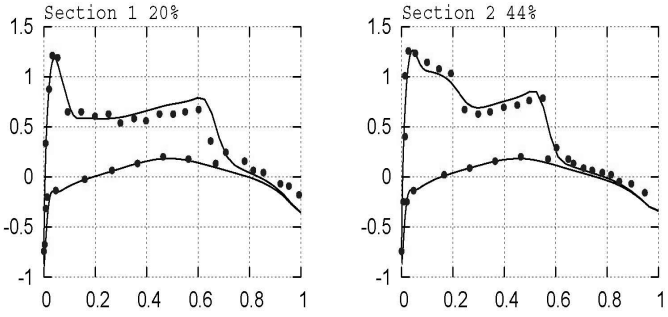

Figure 6a. C_P distribution at 20% and 44% of wing span.

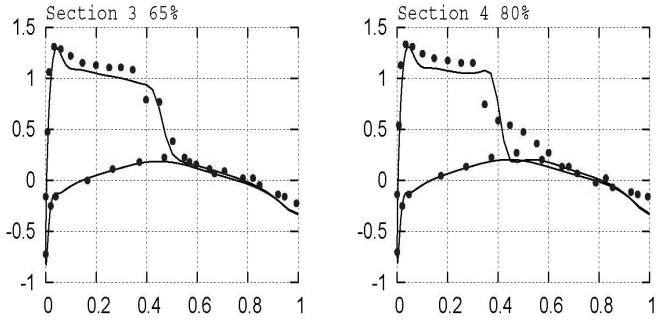

Figure 6b. C_P distribution at 65% and 80% of wing span.

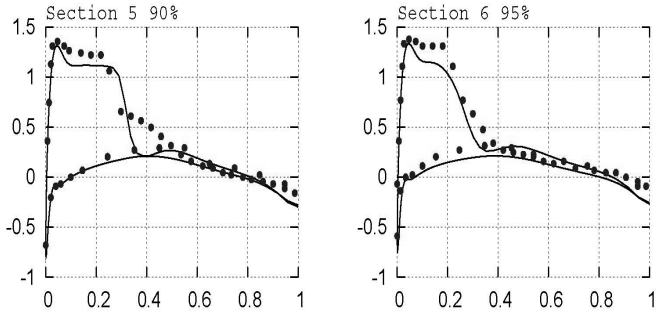

Figure 6c. C_P distribution at 90% and 95% of wing span.

Grid	C_L	C_D	$Time_{consumption}$
96×12×16 200 × 100	*0.4383*	*0.0433*	*69.45s*
82×12×16 200 × 100	*0.4373 0.2%*	*0.0434 0.2%*	*55.83s*
68×12×16 200 × 100	*0.4357 0.5%*	*0.0434 0.2%*	*46.48s*
48×12×16 200×100	0.4372 0.2%	0.0436 0.7%	37.38s
82×6×8 50×50	0.4416 0.7%	0.0422 3%	7.17s
68×6×8 50×50	0.4416 0.7%	0.0422 3%	5.85s
48×6×8 50×50	0.4443 1.3%	0.0425 1.5%	4.22s

Table 3. Flight conditions.

Concluding the validation study through test 1 and 2, it is shown that the results obtained by FLO22 are in good agreement with experimental data. FLO22 has capabilities to provide accurate results and solve the aerodynamic characteristics for 3D wings operating at transonic speeds. FLO22 provides some advantages: The first benefit is good accuracy even considering the inviscid flow assumption. The other advantage when compared full Navier-Stokes solver is the computational time; a single computation takes only 50~70 seconds on a computational grid of 96 × 12 × 16 with 200 iterations. Therefore, the authors have confidence on the capabilities of the solver for its coupling with the optimiser.

After some tests with different grid size, it has been chosen for hierarchical topology as illustrated in table 3; the maximum grid size (96 × 12 × 16 with 200×100 iterations) will applied at first layer as precise model. The medium (82 × 12 × 16 with 200×100 iterations) and lower (68 × 12 × 16 with 200×100 iterations) grid size are applied for the second and third layers respectively. Their results are less 0.5% accuracy difference and much faster when compared to the results from precise model. In addition, the maximum iterations (200 × 100) are also chosen for hierarchical structures since the configuration of model becomes complicated the result obtained from low iteration can not rely on.

V. Practical Test Cases

A. Formulation of the Problem

For the optimisation, Joint Unmanned Combat Air Vehicles (J-UCAVs) are initially considered such as Boeing X-45C, Dassault Aviation - Petit Duc and Northrop Grumman X-47A/B. Due to their confidential wing configurations, the baseline UCAV is similar to the UCAV design project in Reference 34 and illustrated at Fig. 12.

For stealth purposes, the wing planform shape is assumed as an aero-diamond shape with jagged trailing edge which is convenient for deflecting radar echoes away from the source[15, 28]. The aircraft maximum gross weight is approximately 5,190 lb and empty weight is 3,249 lb. The design characterises for the baseline wing configuration are illustrated in table 6. The inboard and outboard sweep angles are 55 degrees. Inboard and outboard taper ratios are 0.68. These identical sweep angles and taper ratios are made a planform alignment that the leading edge is parallel with trailing edge.

The authors also assume that this baseline design contains two types of aerofoils as illustrated in table 7; NACA 67-1015 and NACA 66-008 are applied for the inboard and outboard sections as shown in figures 14, 15 and 16. The aerofoils between inboard and outboard sections are interpolated automatically by the flow solver.

AR	b	Λ_{R-B1}	Λ_{B1-B2}	Λ_{B2-T}	λ_{R-B1}	λ_{B1-B2}	λ_{B2-T}
1.65	18.2	55°	55°	55°	0.68	0.68	0.02

Table 6. Baseline UCAV wing configurations.

Sections	Type of aerofoil
Root	NACA 67-1015
Break Point 1	NACA 67-1015
Break Point 2	NACA 66-088
Tip	NACA 66-088

Table 7. Baseline UCAV aerofoil sections.

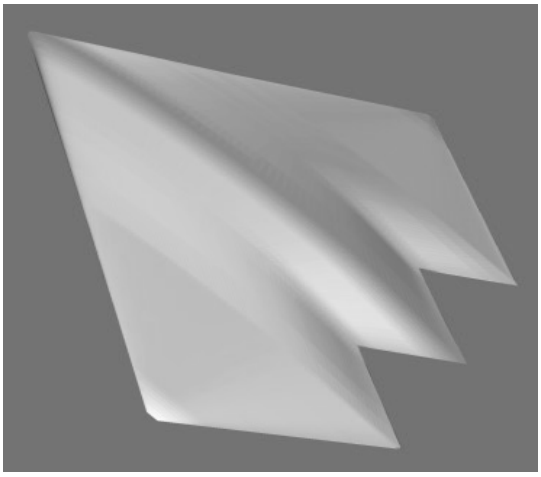

Figure 12. Baseline design for UCAV.

UCAVs are autonomous aircraft that provide commanders the capability to conduct reconnaissance, intelligence, surveillance, and target acquisition (RISTA); battle damage assessment (BDA); and special operations missions. In this paper, RISTA is considered as illustrated in Fig. 13. Initially, it climbs up to 40,000 *ft* then cruise close to the target range at $M_\infty = 0.7$. It will do stealthy ingress to the target point at $M_\infty = 0.9$ and Altitude = 250 *ft* and then destroy target or surveillance target range. At the conclusion of a mission, the UCAV returns to a predetermined location.

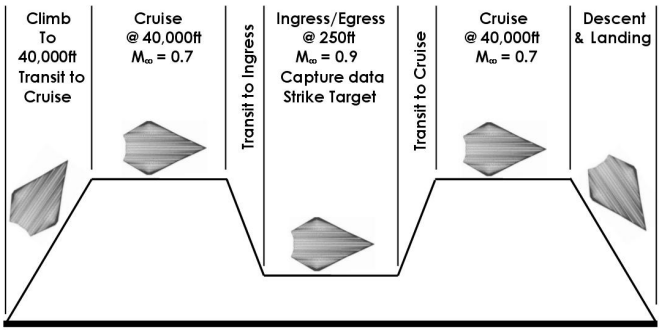

Figure 13. Mission profile for baseline UCAV.

In the optimisation, two flight conditions including the cruise flight condition and ingress flight conditions are investigated. These baseline flight conditions are illustrated in table 8. For the cruise/ingress flight condition, the lift coefficients are calculated 0.1914 and 0.0215. These C_L values are applied as inequality constraints. To achieve these lift coefficients, it was found that the angle of attack should be at 5.408° and 0.5733° respectively.

Variables	M_∞	*Altitude*	$L/D_{Baseline\ Geometry}$
Flight condition 1	0.7	40,000 ft	16.565
Flight condition 2	0.9	250 ft	4.729

Table 8. Flight conditions.

B. Optimisation Rationale and Algorithms

The general optimisation rationale is indicated in algorithm 1 and 2. The algorithm 1 describes the overall optimisation process how it starts with and when it stops. The design process and computation of UCAV are illustrated in algorithms 2 that combine to hierarchical topology.

1) Algorithm I

The algorithm 1 starts with defining the design variables, design constraints, desired flow conditions and fitness functions. An initial population of wing geometries which is pre-described in hierarchical topology layers is randomly generated. The optimiser will run until the termination conditions meet. The algorithm generates candidate wing geometries these will be evaluated with the computational model corresponding to the hierarchical node to which they belong by using algorithm 2. From the algorithm 2, the values of candidate's fitness are collected and will be evaluated as an individual population or discarded. It is also in this stage where the evolution process (mutation, crossover and selection) as well as computation of and migration of candidate geometries from one population to another occurs. If the problem is multi-objective the algorithm computes the non-dominated solutions otherwise it will only compute the update progress history that shows the track of fitness value along the number of fitness function. The termination criterion is satisfied when the prescribed number of function evaluations is reached or when the fitness value goes below a prescribed number. The last stage is the designation of results such as best-so-far individual or non-dominated individuals on the Pareto-front.

2) Algorithm II

Algorithm 2 illustrates the process for the wing aerofoil sections and planform shape design. It is a part of the algorithm 1 and used to generate an initial population and compute the off-strings. The algorithm starts with collection the information of design variables and then the node of hierarchical topology will be determined from the optimiser. The information of node contains the number of aerofoil coordinates points and the grid size of wing geometry. The shape of aerofoil will be determined by Bézier curve function that based on the design variables of the aerofoil sections consist of the mean line and thickness control points. The Bézier functions provide parametric curves and this is useful

to define the shapes and surfaces. The *x* and *y* coordinates of Bezier points are depend on the node of hierarchical topology that is controlled by the methodology. For the wing design variables, sweep angles, taper ratios and the break points are considered. The wing geometry which based on grid size from hierarchical topology is generated and computed using FLO22 and FRICTION at the desired flow condition. The aerodynamics characteristics are obtained and then the fitness functions are computed.

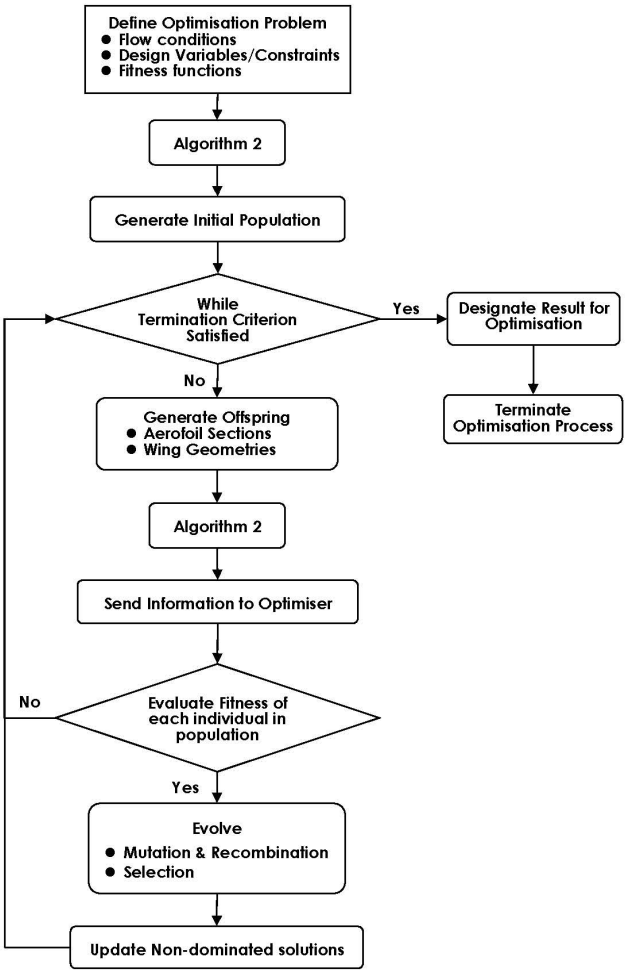

Algorithm 1. Overall optimisation process.

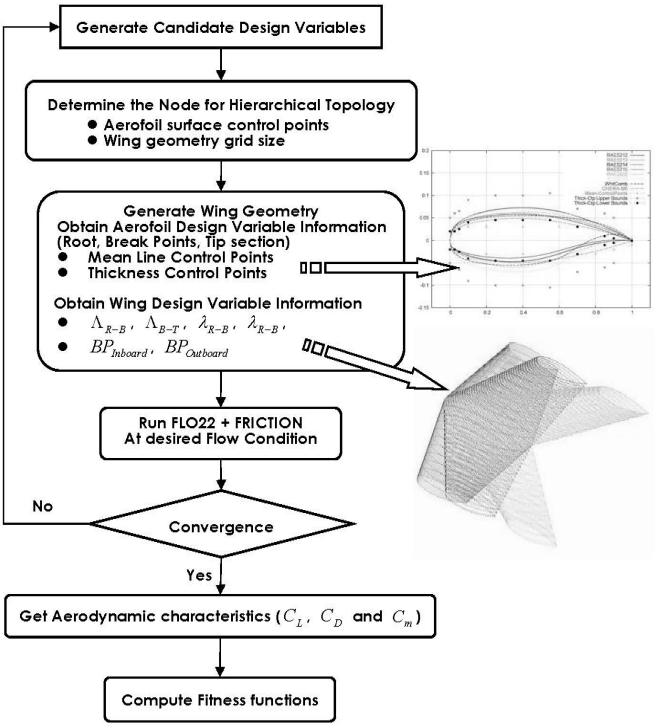

Algorithm 2. Wing aerofoil sections/planform optimisation.

C. Representation of Design Variables

In most of the test cases considered in this paper, the aerofoil geometry is represented using Bézier curves with a combination of a mean line and thickness distribution. This is very common concept in classical aerodynamics[4]. For mean and thickness control points, x coordinates are fixed in advance and y coordinates are controlled by methodology. The design bounds of mean and thickness control points are illustrated in Fig. 14, 15 and 16 with upper right hand corner legends.

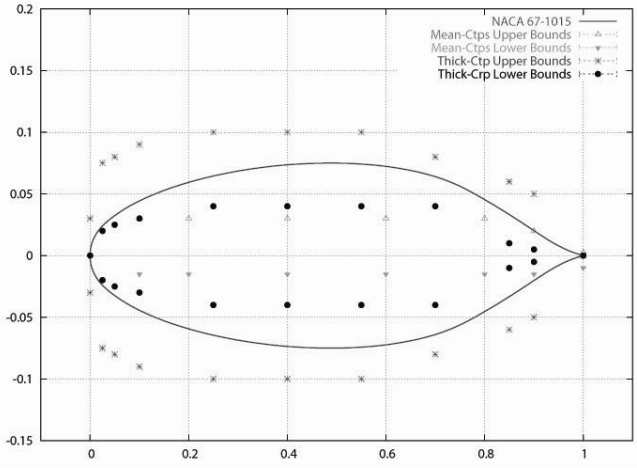

Figure 14. Root mean line and thickness control points.

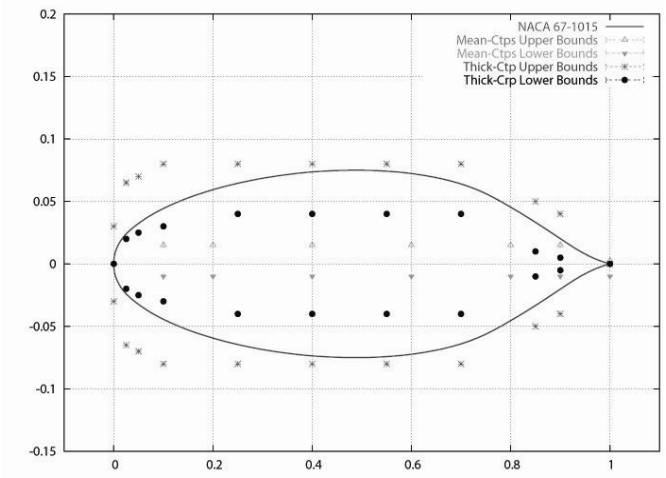

Figure 15. Break Point 1 mean and thickness control points.

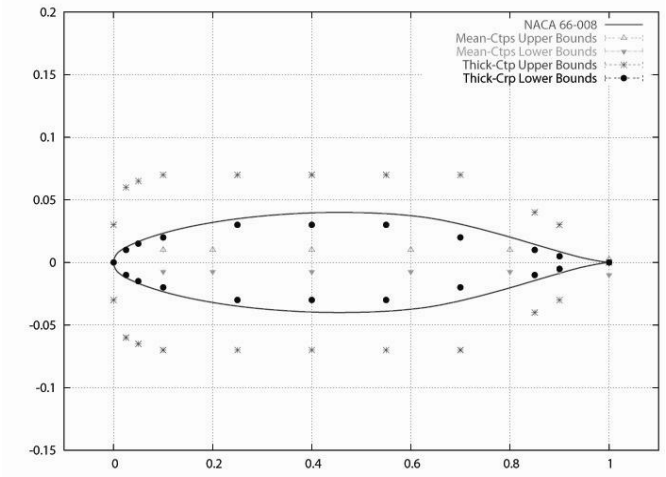

Figure 16. Break Point 2 and Tip mean and thickness control points.

Where X and *Y*-axis represent the chord length and thickness respectively. Figure 14 represents the root section aerofoil design bounds and the bounds of beak point1 aerofoil are shown in Fig. 15. Figure 16 illustrates the design bounds of beak point 2 and tip section aerofoil. The aerofoils will be generated and applied in each spanwise position as illustrated in Fig 11. As wing design variables, three sweep angles, three taper ratio and two break positions are considered to generate wing model.

The wing planform shape is parameterised by considering the variables described in Fig. 17. Three different taper ratios and three sweep angles are considered as planform design variables. In second and third test case, break points (BP1 and BP2) are recomputed to maintain the wing wet area. The length of span is also recalculated.

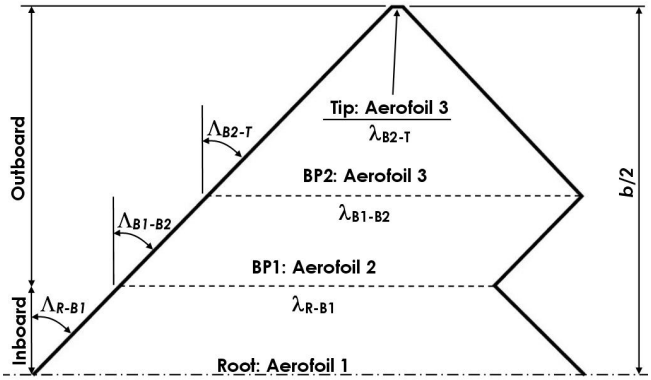

Figure 17. UCAV aerofoil sections and planform design variables.

Three test cases are considered and the summary of test is illustrated in table 9;

Test Case 1	***Aerodynamic design & optimisation of UCAV wing aerofoil sections***
Objectives	Maximise *L/D* at cruise and ingress flight conditions
Design parameters	• Maintain the Original wing planform geometry. • Replacement of aerofoil sections.
Test Case 2	***Aerodynamic design & optimisation of UCAV wing aerofoil sections and planform.***
Objectives	• Maximisation *L/D* at cruise and ingress conditions. • Minimisation *bending moment at ingress conditions* .
Design parameters	• Maintain UCAV wetted area. • Replacement of inboard/outboard taper ratios, break points and sweep angles. • Replacement of aerofoil sections.
Test Case 3	***Aerodynamic and RCS Design and Optimisation of UCAV wing aerofoil sections and planform.***
Objectives	• Maximisation *L/D* at cruise and ingress conditions. • Minimisation *RCS.*
Design parameters	• Maintain UCAV wetted area. • Replacement of inboard/outboard taper ratios, break points and sweep angles. • Replacement of aerofoil sections.

Table 9. Summary of test cases.

D. Test Case 1: Aerodynamic design & optimisation of UCAV Wing Aerofoil Sections.

1) Problem Definition

This first case considers the design and optimisation of the aerofoil sections of a UCAV while keeping the original planform shape constant. The main objectives are to maximise the lift to drag ratio at two operating points and at

fixed angle of attack. The fitness functions with and flight conditions are:

$$fitness(f_1) = \min(1/(L/D_1)),\ C_{L_1} \geq 0.1914$$
$$\rightarrow\ M_\infty = 0.7 \text{ and } \alpha = 5.408°$$
$$fitness(f_2) = \min(1/(L/D_2)),\ C_{L_2} \geq 0.0215$$
$$\rightarrow\ M_\infty = 0.9 \text{ and } \alpha = 0.5733°$$

2) Design Variables

This problem is subject only to side constraints on the design variables. The upper and lower bounds for the aerofoil design variables are illustrated in Fig. 8, 9 and 10. Seven control points are taken on the mean line and ten control points are taken for the thickness distribution respectively.

3) Implementation

The hierarchical topology approach is utilised. The hierarchical models take different computational expense due to different resolutions. After a few test cases, it was found that the following population size and grid size make a good balance on the computational efficiency and accuracy of the results. The following parameters are used on the FLO22 solver and the evolutionary optimiser.

First Layer: Population size of 15 and a computational grid of 96 × 12 × 16 cells.

Second Layer: Population size of 40 and a computational grid of 82 × 12 ×16 cells.

Third Layer: Population size of 60 and a computational grid of 68 × 12 × 16 cells.

4) Results

The algorithm was allowed to run for approximately 1730 function evaluations and took 200 hours on a single 1.8 *GHz* processor. Fig. 18 illustrates the resulting Pareto non-dominated solutions that are compared to baseline (circle dot) plotted in a little box since is a big improvement at ingress operating condition (*fitness 2*). The lift coefficient distribution for each member of the Pareto front is shown in figures 19 and 20. A higher lift coefficient distribution is observed for all Pareto members as compared with the initial design. Pareto member 1, 3, 4 and 15 are selected from the Pareto front to compare their aerodynamic performances are indicated in table 5. Pareto member 3 and 4 are selected for further evaluation since they evenly improved the aerodynamic performance at cruise and ingress conditions when compared to other Pareto members. The aerofoil sections for these Pareto members are compared to the initial design in Fig. 21 and table 11. It can be seen that classical aerodynamic shapes for transonic speeds have been evolved, even considering that the optimisation was started completely at the random and the evolution algorithm had no problem specific knowledge of appropriate solution type. In addition, the aerofoils for the root and break point 1 have a less max-thickness compared to initial design, however for the break point 2 and tip, the thickness of aerofoil is higher than the initial design. The positive cambers are observed at root, break point 1, break point 2 and tip aerofoil. The spanwise pressure distribution between initial design and compromised solutions are shown in Fig. 22 and 23 for the cruise and ingress flight conditions respectively. From these figures, it can be seen that the aerofoil sections for these two geometries are shock free at both flight conditions and consequently the resulting geometries are supercritical wing.

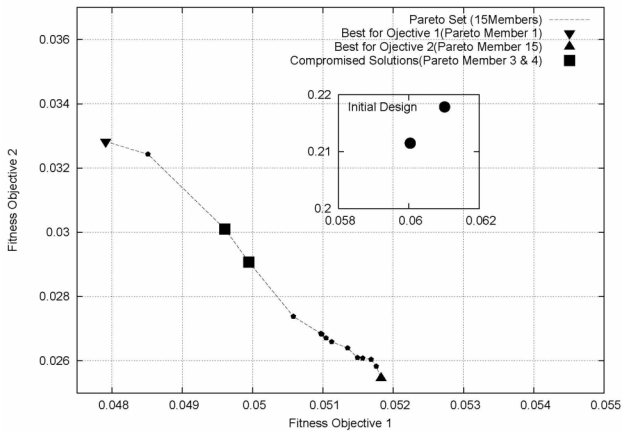

Figure 18. Pareto optimal fronts for UCAV wing aerofoil sections.

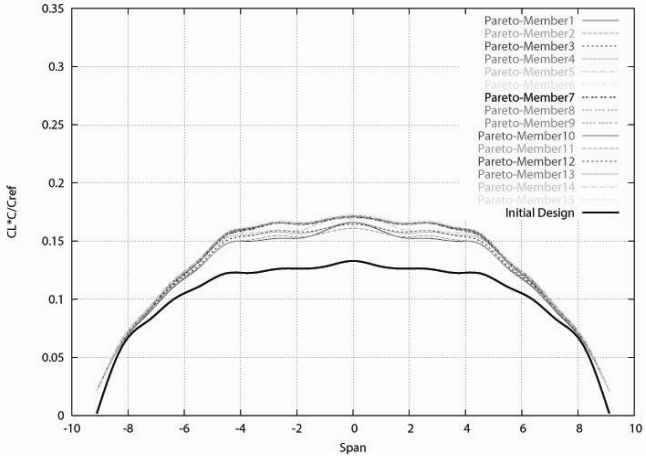

Figure 19. Lift coefficient distribution - Cruise.

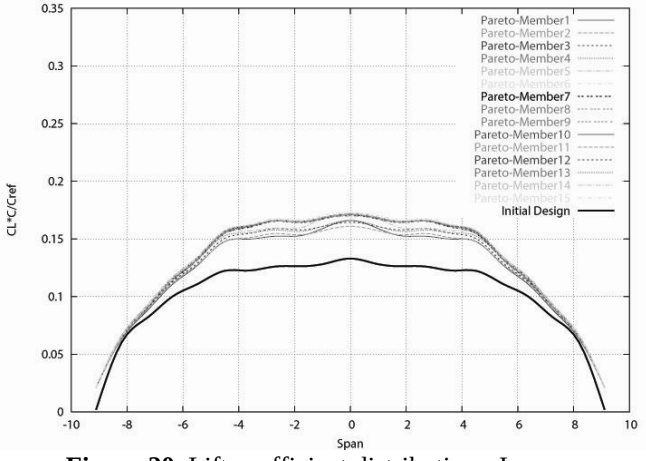

Figure 20. Lift coefficient distribution - Ingress.

Description	Initial design	Pareto M1	Pareto M3	Pareto M4	Pareto M15
L/D_{Cruise}	16.565	20.872	*20.159*	*20.021*	19.295
$L/D_{Ingress}$	4.728	30.464	*33.221*	*34.395*	39.285

Table 10. Comparison of the aerodynamic performance.

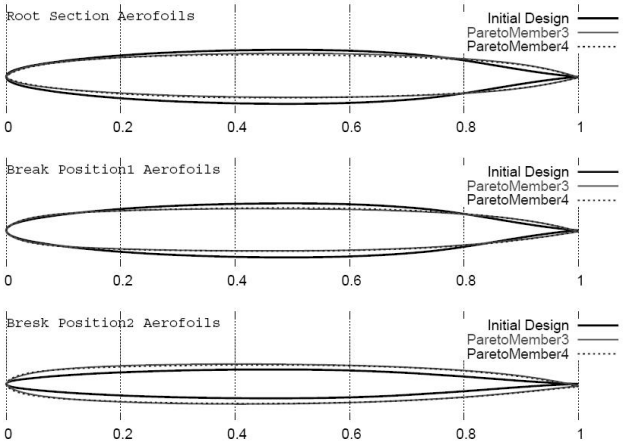

Figure 21. Aerofoils sections for the compromised solutions.

Description (%chord)	Baseline	Pareto M3	Pareto M4
Root *Thick(Camber)*	15.0(0.0)	12.2(0.49)	12.0(0.41)
BreakPoint1 *Thick(Camber)*	15.0(0.0)	11.7(0.51)	12.0(0.44)
BreakPoint2-Tip *Thick(Camber)*	8.0(0.0)	11.10(0.48)	10.8(0.58)

Table 11. Comparison of the aerofoil configurations.

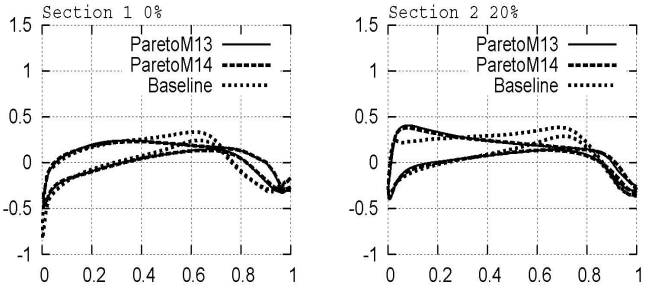

Figure 22a. *Cp* distribution 0 and 20 % - Cruise.

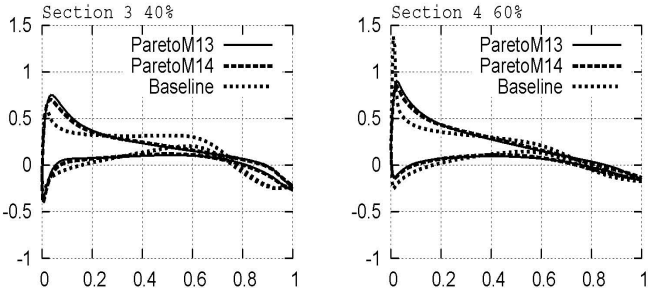

Figure 22b. *Cp* distribution 40 and 60 % - Cruise.

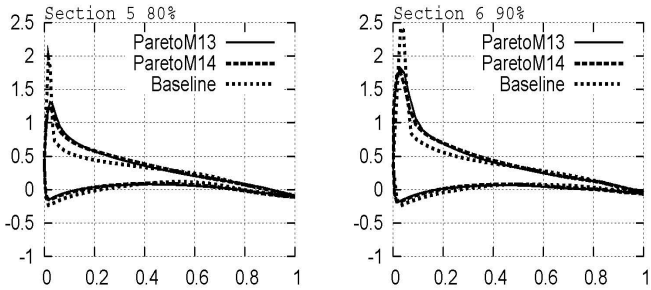

Figure 22c. *Cp* distribution 80 and 90 % - Cruise.

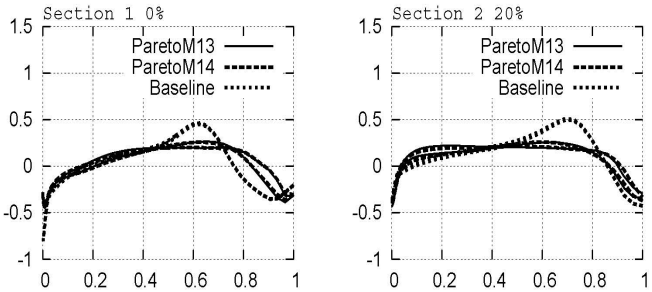

Figure 23a. *Cp* distribution 0 and 20% - Ingress.

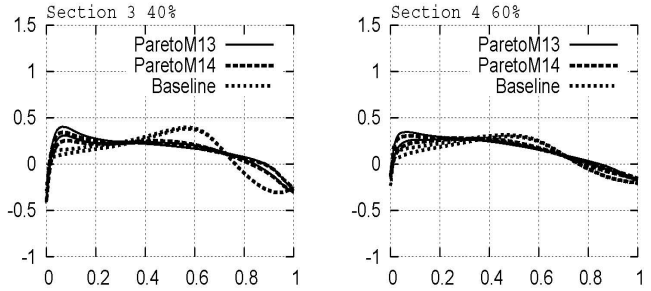

Figure 23b. *Cp* distribution 40 and 60% - Ingress.

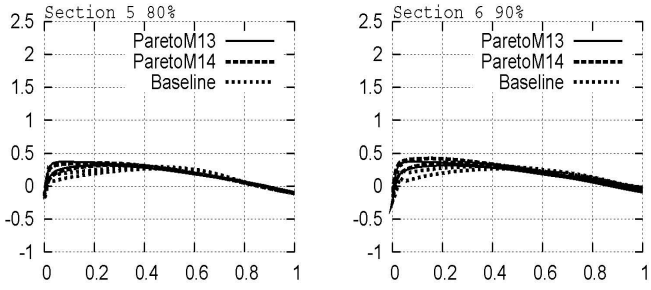

Figure 23c. *Cp* distribution 80 and 90% - Ingress.

E. Test Case 2: Aerodynamic design & optimisation of UCAV Aerofoil Sections/Planform

1) Problem Definition

This test case considers the design and optimisation of a UCAV wing aerofoil sections and planform geometry operating at cruise and ingress conditions. This is a three objectives problem where the objective is to optimise an UCAV wing to produce a high lift to drag ratio at two flight conditions and a low bending moment at ingress conditions. The fitness function and flight conditions are:

$$fitness(f_1) = \min\left(1/(L/D_1)\right),\ C_{L_1} \geq 0.1914$$
$$\rightarrow\ M_\infty = 0.7 \text{ and } \alpha = 5.408°$$
$$fitness(f_2) = \min\left(1/(L/D_2)\right),\ C_{L_2} \geq 0.0215$$
$$\rightarrow\ M_\infty = 0.9 \text{ and } \alpha = 0.5733°$$
$$fitness(f_3) = \min\left(Cm_{bending}\right)$$
$$\rightarrow\ M_\infty = 0.9 \text{ and } \alpha = 0.5733°$$

2) Design Variables

Only the side constraints are considered for the design variables. The design variables are for the aerofoil sections at three spanwise stations as described in Fig. 14, 15 and 16. For the wing planform design, six design variables are considered including $\lambda_{R\text{-}B1}$, $\lambda_{B1\text{-}B2}$, $\lambda_{B2\text{-}T}$, $\Lambda_{R\text{-}B1}$, $\Lambda_{B1\text{-}B2}$ and $\Lambda_{B2\text{-}T}$. To maintain the same wing wetted area as initial design, and break point positions are recalculated without twist and dihedral factors. The upper and lower design bounds are illustrated in table 12 and Fig. 24.

Variables	λ_{R-B1}	λ_{B1-B2}	λ_{B2-T}	Λ_{R-B1}	Λ_{B1-B2}	Λ_{B2-T}
Lower Bounds	0.6	80 (% λ_{R-B1})	0.002	45°	45°	45°
Upper Bounds	0.9	100 (% λ_{R-B1})	0.1	65°	65°	65°

Table 12. Wing planform design variables.

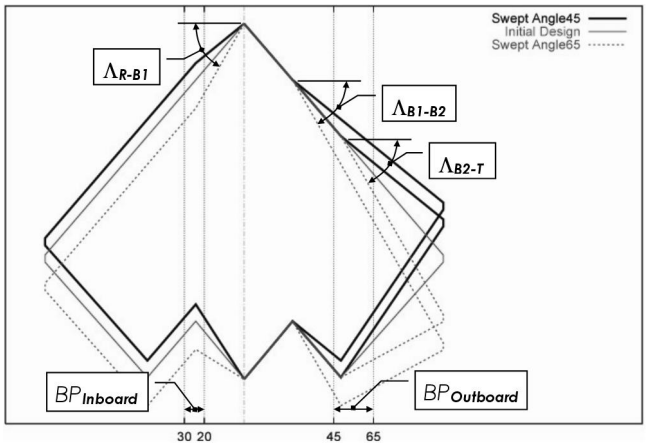

Figure 24. Wing planform shape corresponds to design variables.

3) Implementation

The FLO22 solver is utilised and the following specific parameters are considered for the evolutionary optimiser using a hierarchical topology concepts.

First Layer: Population size of 40 with a computational grid of 96 × 12 × 16 cells.

Second Layer: Population size of 40 with a computational grid of 82 × 12 ×16 cells.

Third Layer: Population size of 60 with a computational grid of 68 × 12 × 16 cells.

4) Results

The algorithm was allowed to run for approximately 1550 function evaluations and took 200 hours on a single 1.8 GHz processor. The resulting Pareto set is shown in figures 25a to 25d. Figures 25b and c show that the data distributions for objective 3 vs. 1 and objective 3 vs. 2 represent convex functions while the data for objective 2 vs. 1 represents linear function. The wing planform shapes corresponding to the Pareto front are illustrated in Fig. 26. The lift coefficient distributions for cruise and ingress conditions are illustrated in Fig. 27 and 28. Fig. 29 shows the bending moment coefficient distribution for the ingress condition. Four Pareto member 1, 13, 14 and 15 are selected to compare the aerodynamic performances to the initial design as indicated in table 13. Pareto member 13 and 14 is selected as compromised solution for further evaluation. The aerofoil sections are compared in Fig. 30 and table 14 where it is observed that the aerofoils for the root and break point 1 stations contain a less max-thickness when compared to initial design aerofoils while the aerofoil for break point 2 and tip station is thicker than initial aerofoil. The negative camber aerofoil is observed at break point 1, break point 2 and tip section while the aerofoil at root section contains the positive camber. The spanwise *Cp* distribution between compromised solutions and initial design for cruise and ingress conditions are compared in figures 31 and 32 where it can be seen that the compromised solution is a supercritical wing. A top, side, front and three-dimensional view for one of optimal wing geometries (Pareto member 14) is illustrated in Fig. 33.

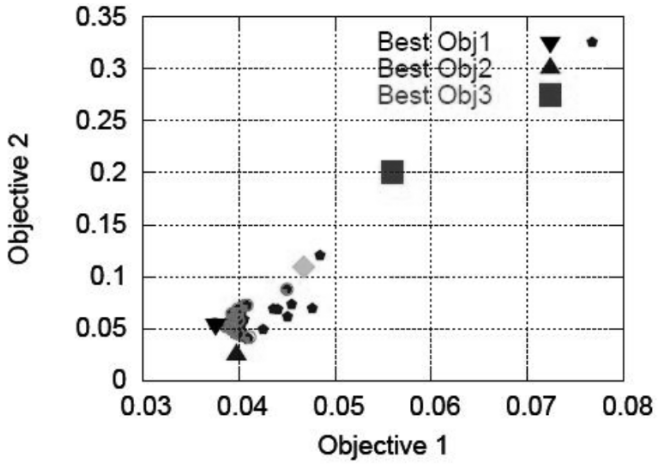

Figure 25a. Non-dominated Pareto fronts objective2 vs objective1.

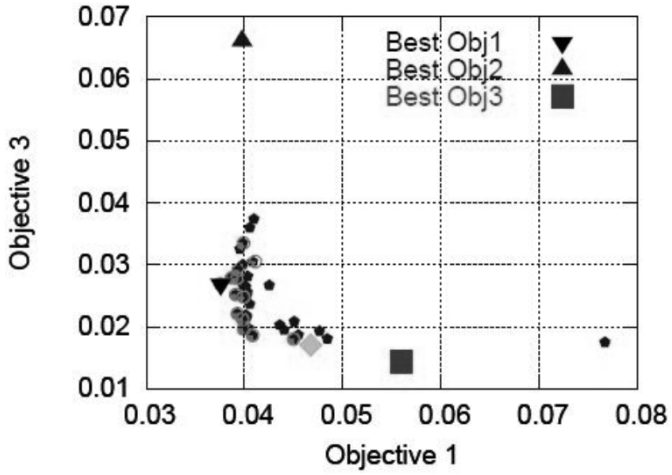

Figure 25b. Non-dominated Pareto fronts objective3 vs objective1.

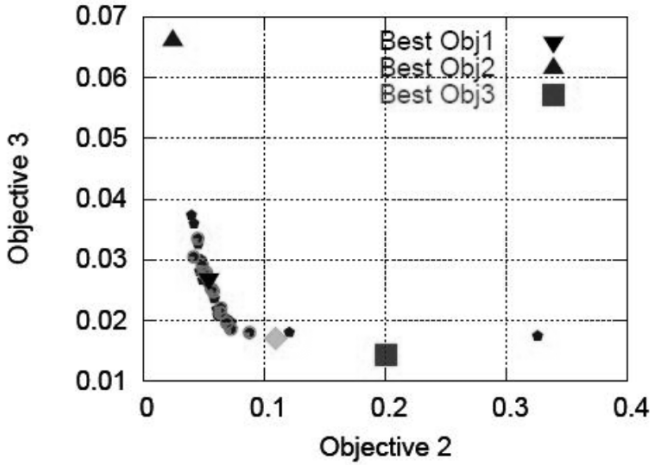

Figure 25c. Non-dominated Pareto fronts objective3 vs objective2.

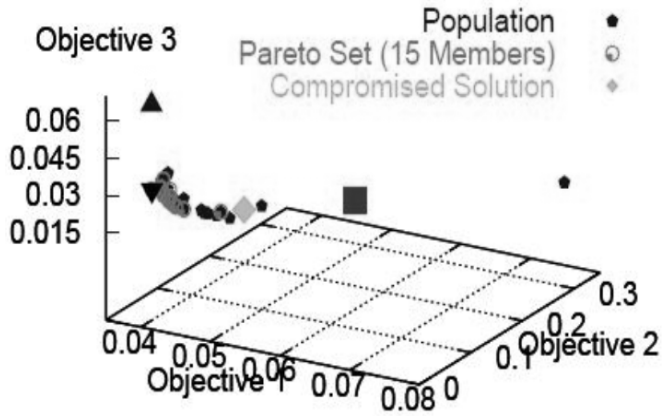

Figure 25d. Non-dominated Pareto fronts for UCAV wing aerofoil sections/planform.

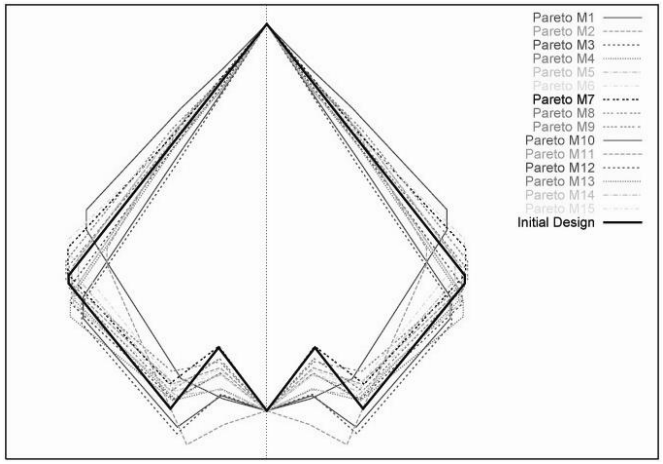

Figure 26. Pareto set planform shapes.

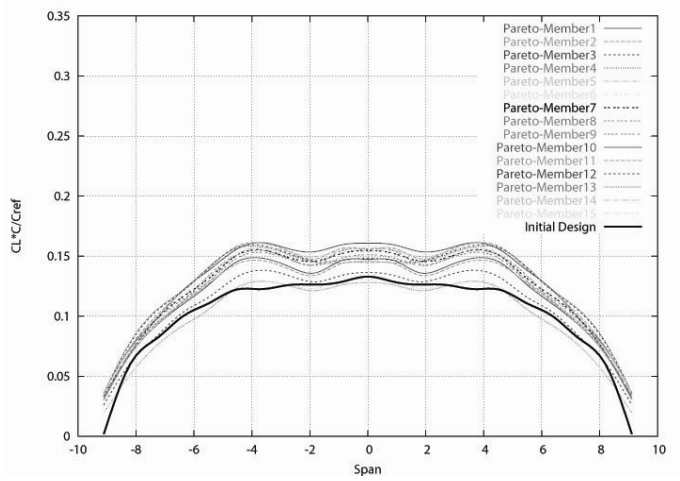

Figure 27. Lift coefficient distribution-Cruise.

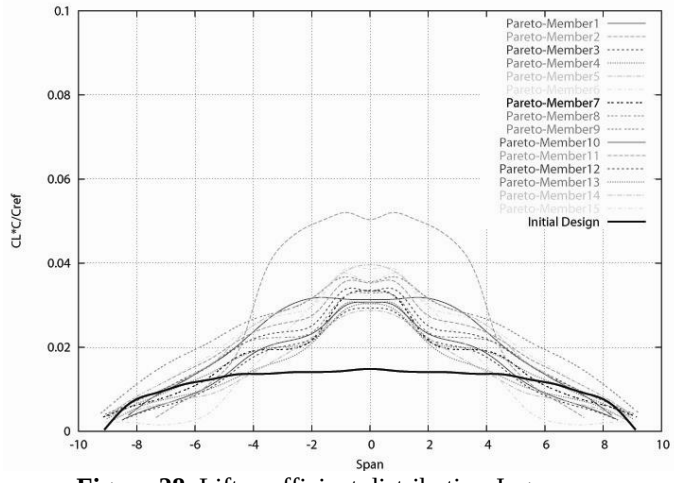

Figure 28. Lift coefficient distribution-Ingress.

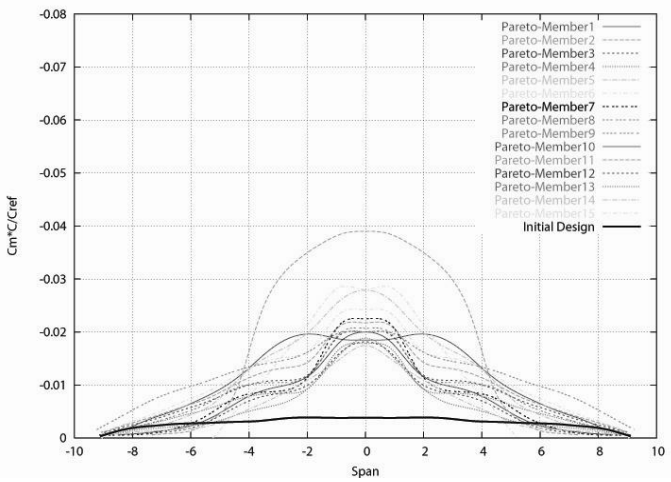

Figure 29. Bending moment distribution-Ingress.

Description	Base line	Pareto M1	Pareto M13	Pareto M14	Pareto M15
L/D_{Cruise}	16.565	26.648	*22.222*	*21.400*	*17.871*
$L/D_{Ingress}$	4.729	18.413	*11.388*	*9.150*	*4.986*
$Cm_{Bending}$	0.0185	0.0269	*0.0180*	*0.0170*	*0.0143*

Table 13. Comparison of the aerodynamic performance.

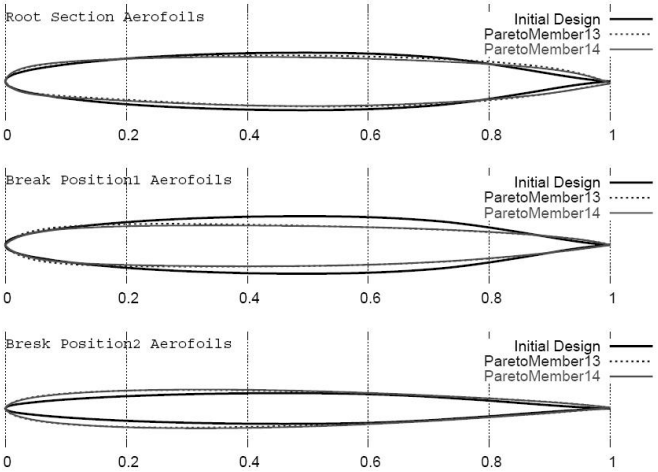

Figure 30. Aerofoils sections for the compromised solutions.

Description (%chord)	Baseline	Pareto M13	Pareto M14
Root *Thick(Camber)*	15.0(0.0)	13.3(0.72)	12.7(0.56)
BreakPoint1 *Thick(Camber)*	15.0(0.0)	11.1(-0.33)	10.6(-0.27)
BreakPoint2-Tip *Thick(Camber)*	8.0(0.0)	9.8(-0.13)	10.1(0.18)

Table 14. Comparison of the aerofoil configurations.

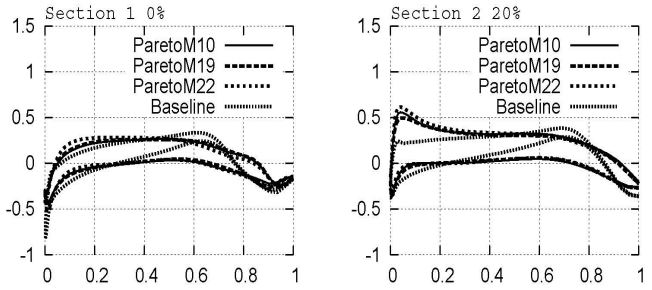

Figure 31a. *Cp* distribution 0 and 20% - Cruise.

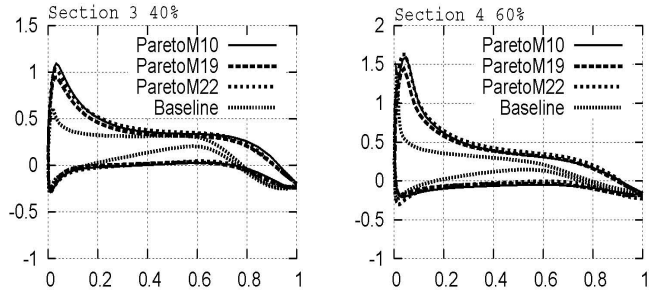

Figure 31b. *Cp* distribution 40 and 60% - Cruise.

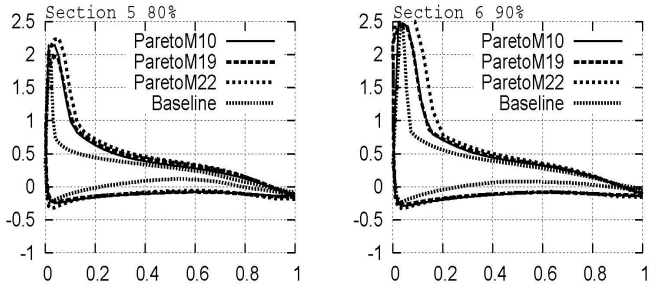

Figure 31b. *Cp* distribution 80 and 90% - Cruise.

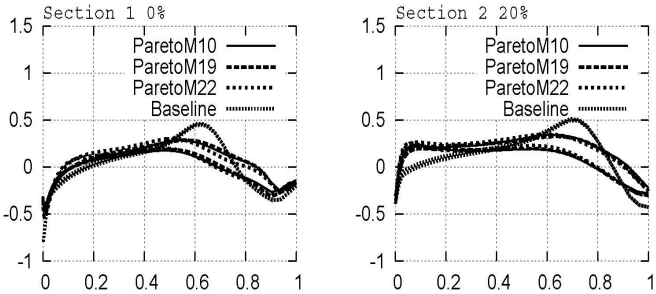

Figure 32a. *Cp* distribution 0 and 20% - Ingress.

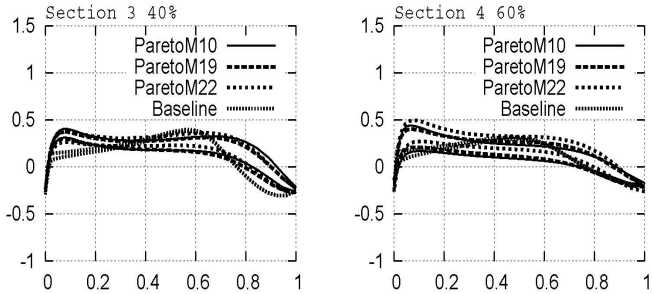

Figure 32b. *Cp* distribution 40 and 60% - Ingress.

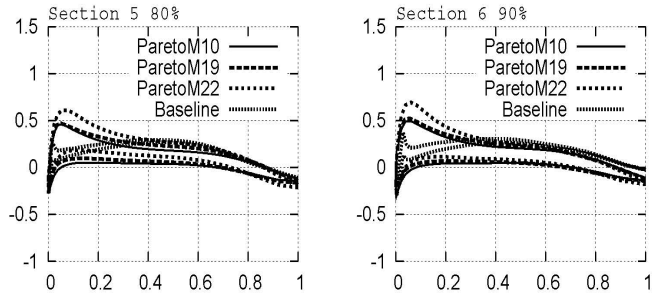

Figure 32c. *Cp* distribution 80 and 90% - Ingress.

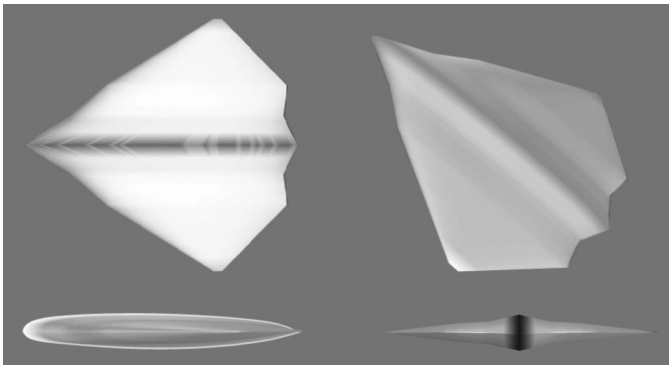

Figure 33. Top/side/front and 3D view for compromised solution (Pareto member 14).

F. Test Case 3: Aerodynamic and RCS design & optimisation of UCAV aerofoil sections and planform

1) Problem Definition

This test case considers the design and optimisation of a UCAV wing aerofoil sections and planform geometry operating at cruise and ingress conditions in addition, one of RCS factors including geometry area is also considered. Radar cross section, σ, is easily visualised as the product of three factors;

$$\sigma = \begin{pmatrix} \text{Geometirc} \\ \text{Cross Sections} \end{pmatrix} \times (\text{Reflectivity}) \times (\text{Directivity})$$

where the area of the target presents to the radar can be referred to geometric cross sections. Reflectivity refers to the fraction of the intercepted power that is reflected by the target, regardless of direction. Directivity is related to reflectivity but refers to the power scattered back in the direction of the transmitting radar.

In this test, the authors only considered frontal area of model as a geometric cross section to reduced RCS. The objectives are the maximisation of the lift to drag ratios at cruise and ingress conditions while the frontal area is minimised. The fitness function and flight conditions are as followed:

$$fitness(f_1) = \min\left(1/(L/D_1)\right),\ C_{L_1} \geq 0.1914$$
$$@\ M_\infty = 0.7 \text{ and } \alpha = 5.408°$$

$$fitness(f_2) = \min\left(1/(L/D_2)\right),\ C_{L_2} \geq 0.0215$$
$$@\ M_\infty = 0.9 \text{ and } \alpha = 0.5733°$$
$$fitness(f_3) = \min\left(Area_{Frontal}/100\right)$$

2) Design Variables

The design variables are for the aerofoil sections at three spanwise stations as described in Fig. 14, 15 and 16. For the wing planform design, six design variables are considered including $\lambda_{R\text{-}B1}$, $\lambda_{B1\text{-}B2}$, $\lambda_{B2\text{-}T}$, $\Lambda_{R\text{-}B1}$, $\Lambda_{B1\text{-}B2}$ and $\Lambda_{B2\text{-}T}$. To maintain the same wing wetted area as initial design, and break point positions are recalculated without twist and dihedral factors. The upper and lower design bounds are illustrated in table 5.

3) Implementation

The FLO22 solver is utilised and the following specific parameters are considered for the evolutionary optimiser using a hierarchical topology concepts.

First Layer: Population size of 200 with a computational grid of 96 × 12 × 16 cells.

Second Layer: Population size of 40 with a computational grid of 82 × 12 ×16 cells.

Third Layer: Population size of 60 with a computational grid of 68 × 12 × 16 cells.

4) Results

The algorithm was allowed to run approximately for 1600 function evaluations and took 200 hours on a single 1.8 *GHz*. The resulting Pareto set is shown in figure 34. Figure 34 shows that the data distribution for objective 1and 2 represent a linear function.

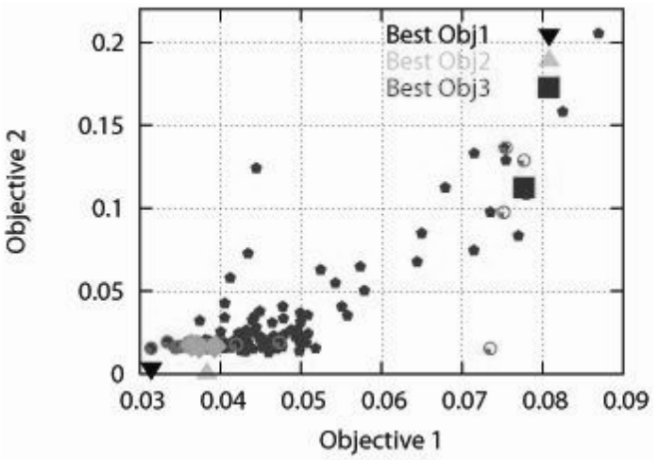

Figure 34a. Non-dominated Pareto fronts objective2 vs objective1.

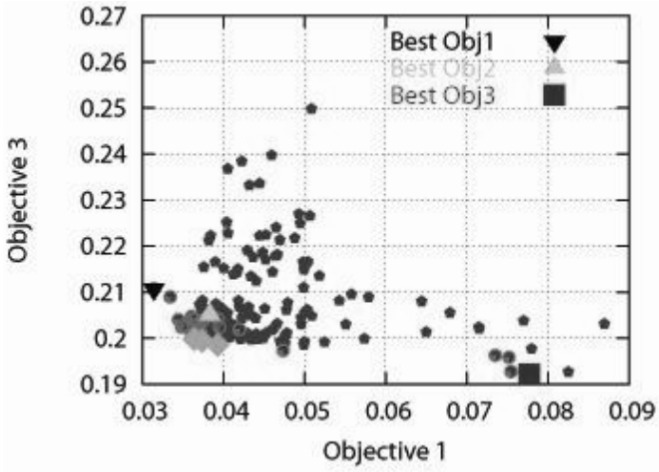

Figure 34b. Non-dominated Pareto fronts objective3 vs objective1.

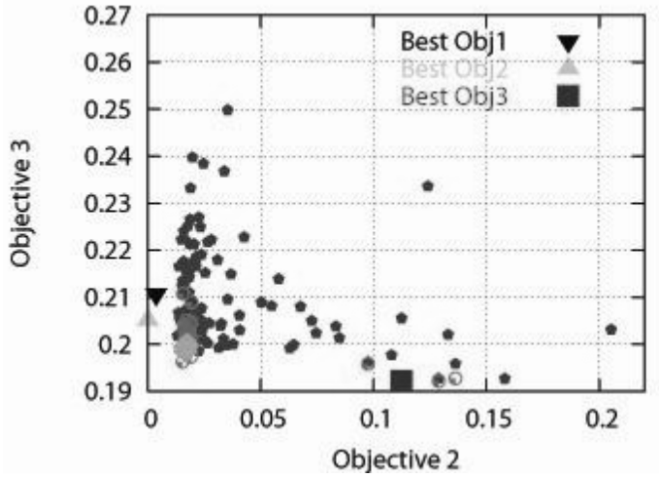

Figure 34c. Non-dominated Pareto fronts objective3 vs objective1.

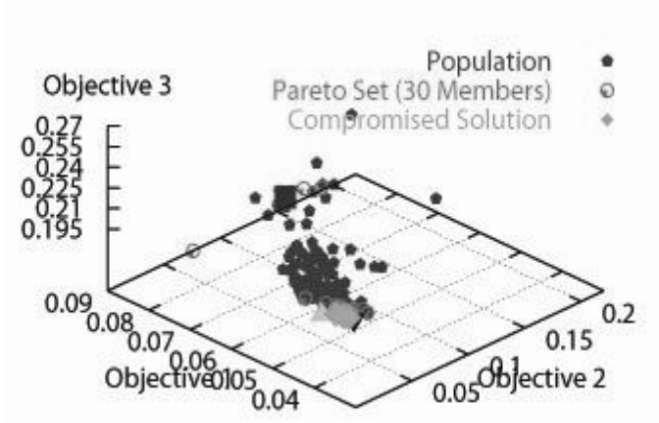

Figure 34d. Non-dominated Pareto fronts for UCAV aerodynamic and RCS

The wing planform shapes corresponding to the Pareto front are illustrated in figure 35 where it can be seen that most of non-dominated solutions contain an arrow shape of wing geometry beside aero-diamond planform. The lift coefficient distribution of Pareto set for cruise and ingress conditions are illustrated in figures 36 and 37. Five members (1, 10, 19, 22, 30) of the Pareto front are selected to compare the aerodynamic performance in table 15. Their wing configurations are compared to initial design in table 16 where it can be seen that the aspect ratio becomes almost double. Pareto member 10, 19 and 22 are selected for further evaluation since, they produce higher ratio of lift to drag for both cruise and ingress conditions and contain lower frontal area by 14% when compared to the initial design in other word, this leads lower RCS. The aerofoil sections are compared in figure 38 and table 17 where it can be seen that the aerofoils for the root and break point 1 have a less max-thickness compared to initial design, however for the break point 2 and tip, the thickness of aerofoil is higher and the positive cambers are observed. The spanwise *Cp* distribution between compromised solutions and initial design for cruise and ingress conditions are compared in figures 39 and 40 where the compromised solutions are the supercritical wings at ingress conditions. Top, side and three-dimensional views for non-dominated solution wing geometry (Pareto member 22) is illustrated in figures 41. In addition, their wing geometries are quite similar to the stealth fighter F-117 Nighthawk as shown in figure 42.

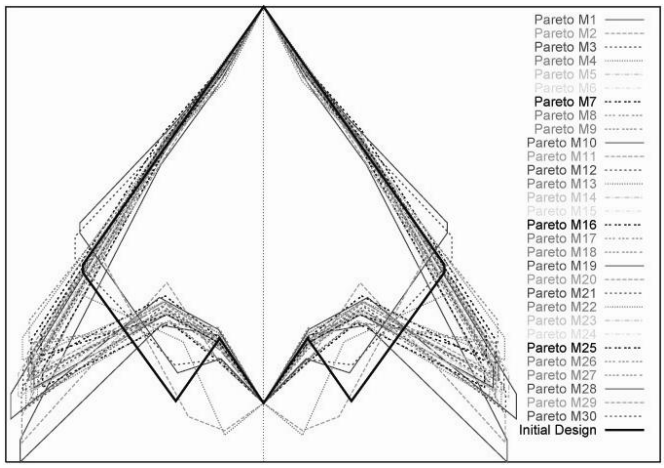

Figure 35. Pareto set planform shapes.

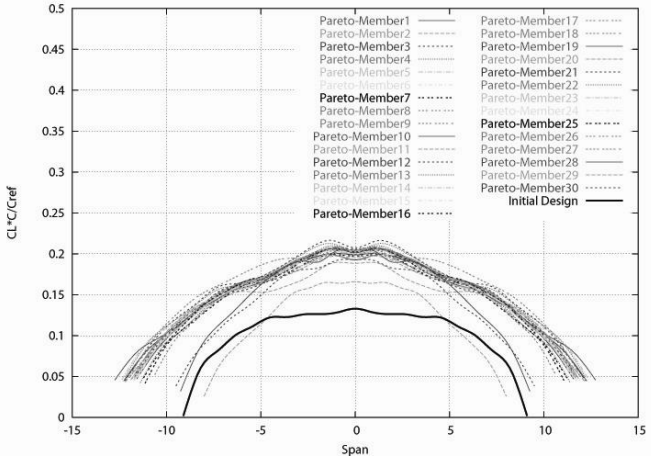

Figure 36. Lift coefficient distribution-Cruise.

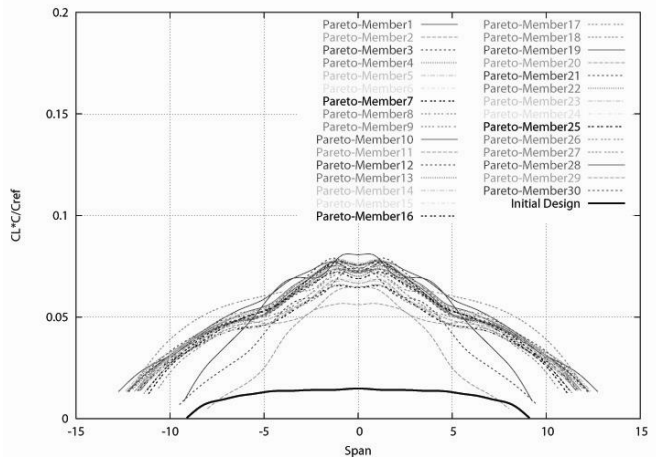

Figure 37. Lift coefficient distribution-Ingress.

Description	Base line	Pareto M1	Pareto M10	Pareto M19	Pareto M22	Pareto M30
L/D_{Cruise}	16.56	31.85	*27.48*	*26.78*	*25.46*	12.87
$L/D_{Ingress}$	4.729	63.88	*57.25*	*61.03*	*60.10*	7.76

Table 15. Comparison of the aerodynamic performance.

Description	Base line	Pareto M1	Pareto M10	Pareto M19	Pareto M22	Pareto M30
$Area_{Front}$	23.28	21.08	*19.98*	*20.11*	*20.15*	19.28
AR	1.66	3.02	*3.25*	*2.68*	*2.96*	1.80
Span	18.22	24.55	*25.49*	*23.15*	*24.32*	18.99

Table 16. Comparison of wing configurations.

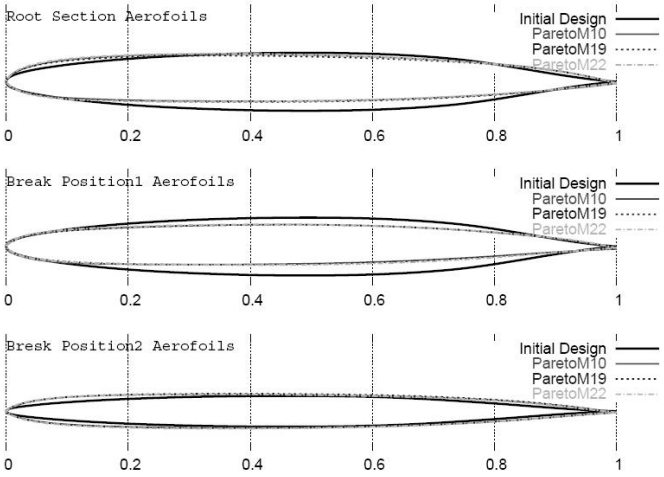

Figure 38. Aerofoils sections for the compromised solutions.

Description (%chord)	Baseline	PM10	PM19	PM22
Root *Thick(Camber)*	15.0(0.0)	12.(1.21)	12.0(0.89)	12.5(1.18)
BreakPoint1 *Thick(Camber)*	15.0(0.0)	10.3(1.11)	10.3(1.0)	10.5(0.75)
BreakPoint2-Tip *Thick(Camber)*	8.0(0.0)	8.7(0.38)	8.9(0.44)	8.9(0.33)

Table 17. Comparison of the aerofoil configurations.

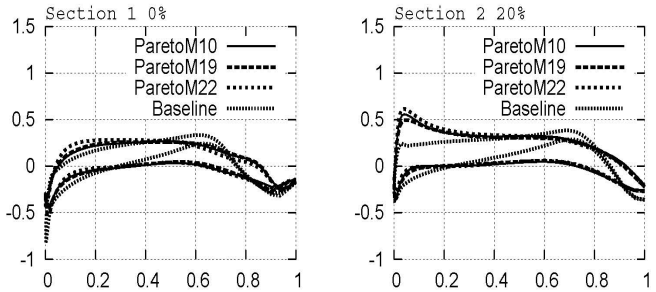

Figure 39a. *Cp* distribution 0 and 20% - Cruise.

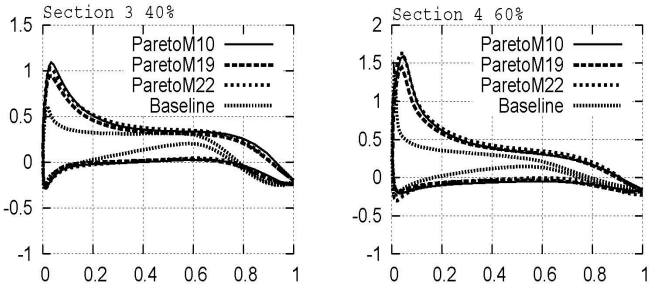

Figure 39b. *Cp* distribution 40 and 60% - Cruise.

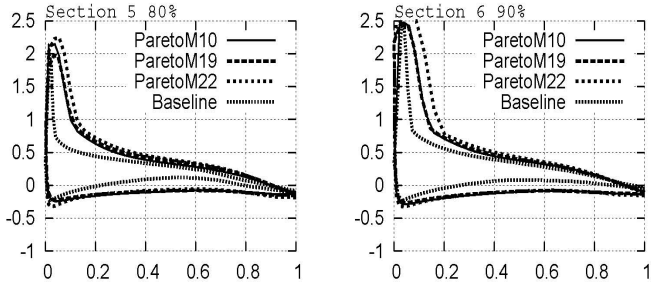

Figure 39c. *Cp* distribution 80 and 90% - Cruise.

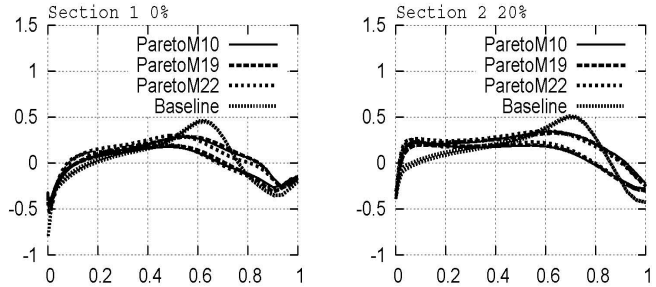

Figure 40a. *Cp* distribution 0 and 20% - Ingress.

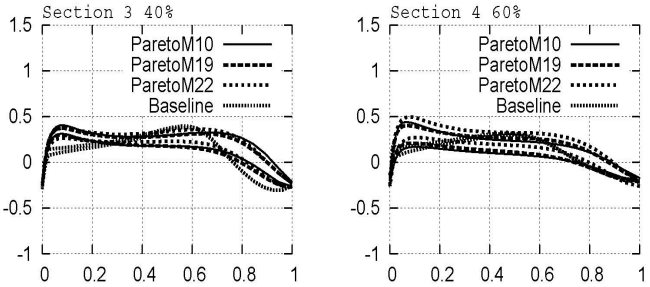

Figure 40b. *Cp* distribution 40 and 60% - Ingress.

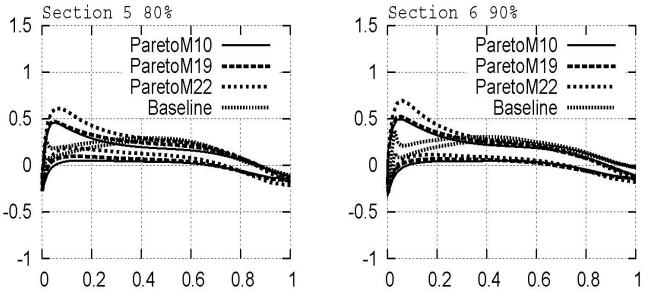

Figure 40c. *Cp* distribution 80 and 90% - Ingress.

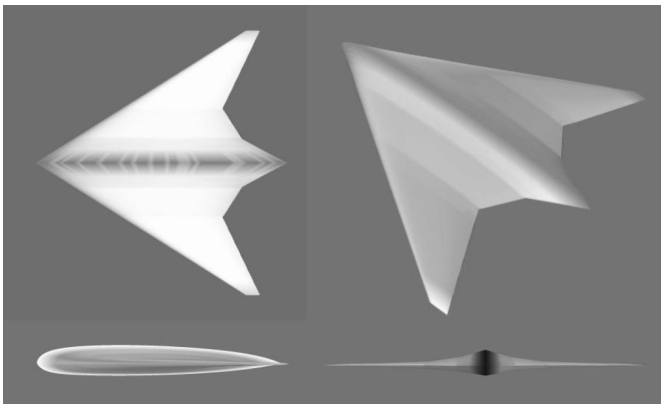

Figure 41. Top/side/front and 3D view for compromised solution (Pareto member 14).

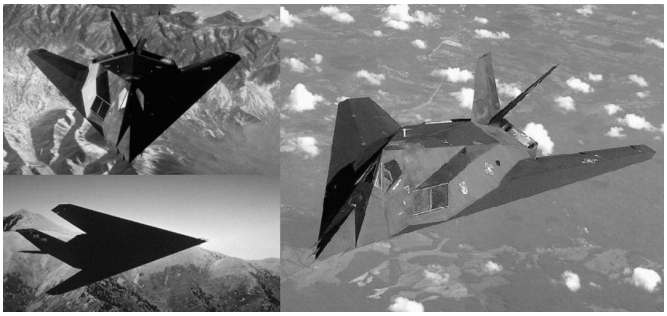

Figure 42. F-117 NightHawk.

VI. Discussion

This paper explored the use applications of HAPMOEA for UAVs and UCAVs. The results from three test cases give still us three discussion points and possible research avenues;

1. *CPU time cost*;

The Hierarchical asynchronous approach is promising but even using low/middle flow solvers, the computations cost is still expensive since the aircraft model has a complex geometry. Another reason for a high computational cost is the multi-objective approach, in the cases evaluated the authors use the Pareto-EAs technique which is effective in find wide range solution by based on Pareto-ranking and sharing but leads to expensive CPU time cost. As further investigation, there are two possible ways to reduce time expense; the physical way by using a cluster of computers. The second is implementing *Nash*[39, 40] (Game Theory).

2. *Design variation*;

Two discussion points on design variation are considered. The first one is related to non-dominated solutions producing a stable aerodynamic performance at two design points. In this paper, two flow conditions; cruise and ingress are considered, this can cause a poor aerodynamic performance at a transition point or slightly off-set conditions. To guarantee the stable and high aerodynamic performance at off-set conditions, the *Uncertainty (Taguchi)*[41] approach should be implemented and compared. The second point is that the three test cases considered aerodynamic performance only without any structural considerations. That can cause an unstable structure. Current work focuses on a multidisciplinary (aero-structure) design optimisation implementation.

3. *RCS solvers*;

In the final test case, the frontal area is minimised to produce low observability aircraft. Even though the non-dominated solutions resemble a stealth aircraft, the requirement of introducing a solver that accounts for the physics is required. Current tests are being conducted using RCS prediction softwares with Maxwell (high fidelity) or physical optic approximation[42].

VII. Conclusion

In this paper, a methodology for the design and optimisation of UAV/UCAV aerofoil sections and wing planform shapes have been described and investigated. The methodology couples a multi-objective evolutionary algorithm and a series of software for aerodynamic analysis for the conceptual and preliminary design of UAV/UCAVs. Results indicate the capabilities of the method to find optimum geometries for UAV/UCAV wing aerofoil sections and planform. Three practical design problems were studied and showed the broad applicability of method. A family of non-dominated Pareto designs obtained from optimisation give the designer a selection so that they may proceed into more detail phases of the design process. Future work will focus on the extension of the concept of the practical design using high fidelity solvers and multi-point design and Radar Cross Section (RCS) reduction.

VIII. Acknowledgements

The authors gratefully acknowledge Dr Eric J. Whitney at Boeing, J. Periaux at INRIA and Mourad Sefrioui Dassault Aviation for the discussions on Hierarchical Asynchronous Parallel EAs, their contribution to the optimisation procedure. Thanks to A. Jamson and David A. Caughey for granting the FLO22 software and W.H. Mason for the use of the FRICTION code.

References

[1] J. Dongarra, W. Jiang, R. Manchek, A. Geist, A. Beguelin and V. Sunderam. *Parallel Virtual Machine: A Users' Guide and Tutorial for Networked Parallel Computing*. Massachusetts Institute of Technology, 55 Hayward Street Cambridge, MA 02142, 1994.

[2] S. Wagner, A. Sommerer, T. Lutz. Numerical optimisation of adaptive transonic airfoils with variable camber. In *Proceedings 22nd ICAS Congress*, number ICA2.111, pages 1-10, Harrogate, United Kingdom, August 27 - September 1. Institute for Aerodynamics and Gas Dynamics, University of Stuttgart, Germany.

[3] D. Quagliarella. A. Vicini. A multiobjective approach to transonic wing design by means of genetic algorithms. In *NATO RTO AVT Symposium on aerodynamic design and optimization*, number RTO-MP-35, Ottawa, Canada, June 2000.

[4] I. H. Abbott and A. E. V. Doenhoff. *Theory of Wing Sections*. Dover, 1980.

[5] D. Allison and W. Sewall. Airfoil modification effects on subsonic and transonic pressure distributions and performance for the EA-6B airplane. Technical Report 3516, NASA, Hampton Virginia, May 1995.

[6] J. Bertin and M. Smith. *Aerodynamics for Engineers*. Prentice-Hall. Inc, 1998.

[7] A. Bolonkin and G. Gilyard. Estimated benefits of variable-geometry wing camber control for transport aircraft. Technical Report TM-206586, NASA, October 1999.

[8] N. Borer. Design and analysis of low Reynolds number airfoils, Industrial Math, Georgia Institute of Technology, December 2002.

[9] K. Deb. *Multi-Objective Optimization Using Evolutionary Algorithms*. Wiley, 2003.

[10] K. Srinivas, E.J. Whitney, M. Sefrioui and J. Periaux. Advances in hierarchical, parallel evolutionary algorithms for aerodynamic shape optimisation. In *JSME International Journal*, volume 45 of *B*. JSME International Journal, JSME International Journal, 2002.

[11] K. Srinivas, J. Periaux, E.J. Whitney, L.F. Gonzalez and M. Sefrioui. Adaptive evolution design without problem specific knowledge: UAV applications. In *Optimisation and Control with Application to Industrial Problems*, Barcelona, Spain, September 2003. EUROGEN.

[12] S. Chen, F. Zhang and M. Khalid. Multi-point optimization of transonic wing by real-coded genetic algorithm. Vancouver, BC, May 28 - 30. CFD2003.

[13] S. Gano and J. Renaud. Optimized unmanned aerial vehicle with wing morphing for extended range and endurance. In *AIAA/ISSMO Symposium and Exhibit on Multidisciplinary Analysis and Optimization*, volume 9. AIAA, 2002.

[14] M. Gen and R. Cheng. *Genetic Algorithm and Engineering Design*. John Wiley and Sons. Inc, New York, first edition, 1997.

[15] L. Gurel and H. Bagci. Validation through comparison: Measurement and calculation of the bistatic radar cross section of a stealth target. *RADIO Science*, 38(3), 3 June 2003.

[16] Hansen, N. and A. Ostermeier, Convergence properties of evolution strategies with the derandomized covariance matrix adaptation $\mu/\mu_I, \lambda)$-ES. In *EUFIT'97, 5th Europ.Congr.on Intelligent Techniques and Soft Computing, Proceedings*, Aachen, pp. 650-654. Verlag Mainz, Wissenschaftsverlag, 1997.

[17] Hansen, N. and A. Ostermeier, Completely Derandomized Self-Adaptation in Evolution Strategies. *Evolutionary Computation*, 9(2), pp. 159-195, 2001.

[18] Hansen, N., S.D. Müller and P. Koumoutsakos, Reducing the Time Complexity of the Derandomized Evolution Strategy with Covariance Matrix Adaptation (CMA-ES). *Evolutionary Computation*, 11(1), pp. 1-18, 2003

[19] J. Hua and F. Kong. Optimization of long-endurance airfoils. In *AIAA Applied Aerodynamics Conference*, volume 21, Orlando, 2003. AIAA.

[20] A. Jameson, D.A. Caughey, P.A. Newman and R.M. Davis, NYU Transonic Swept-Wing Computer Program - FLO22, Langley Research Center, 1975.

[21] P. T. J.P. Hämäläinen, R.A.E. Mäkinen and J.Toivenen. Evolutionary shape optimization in CFD with industrial applications. In *European Congress on Computational Method in Applied Sciences and Engineering*, Barcelona, 11-14 September 2000. ECCOMAS.

[22] J. Koza. *Genetic Programming II*. Massachusetts Institute of Technology, 1994.

[23] K. Srinivas, J. Periaux, L.F. Gonzalez, E.J. Whitney and M. Sefrioui. Multidisciplinary aircraft conceptual design and optimisation using a robust evolutionary technique. In *Proceedings of the 4th European Congress on Computational Methods in Applied Sciences and Engineering*, Finland, July 24-28 2004. ECCOMAS.

[24] T. Lutz. Airfoil design and optimisation. In *GAMM 2000 Conference*, Göttingen, Germany, April 2-7 2000. GAMM.

[25] W. Mason. Applied computational aerodynamics. page Appendix D: Programs, Tuesday, January 21, 1997.

[26] Z. Michalewicz. *Genetic Algorithms + Data Structures = Evolution Programs*. Artificial Intelligence, Springer-Verlag, 1992.

[27] Y. Takeguchi, S. Obayashi and D. Sasaki. Evolutionary comtutation of supersonic wing shape optimisation. In *IEEE Transactions on Evolutionary Computation*, volume 4, pages 182-187. IEEE, July 2000.

[28] U. Samli and N. Cotuk. Shaping considerations in the RCS reduction. 81504 Pendik Istanbul Turkey, 7-8 May 2003. AFCEA.

[29] M. Sefrioui and J. Periaux. Genetic algoriths, game theory and hierarchical models:some theoretical background. In D. G. Periaux, J. and H. v. K. Deconinck, editors, *Genetic Algorithms for Optimization in Aeronautics and Turbomachinery*, Belgium, 2002. Institute for Fluid Dynamics, Institute for Fluid Dynamics.

[30] W. Stadler. *Multicriteria Optimization in Engineering and in the Sciences*. Plenum Press, New York and London, first edition, 1988.

[31] G. Stimon. *Introduction To Airvorne Radar*. SciTech Publishing, Inc, 1998.

[32] J. Wakunda and A. Zell. Median-selection for parallel steady-state evolution strategies. In *PPSN*, pages 405-414, 2000.

[33] E. J. Whitney. *A Modern Evolutionary Technique for Design and Optimisation in Aeronautics*. PhD thesis, The University of Sydney, 2003.

[34] Team Decepticon, Department of Aeronautical & Astronautical Engineering at the University of Illinois. AIAA Undergraduate Design Competition 1998.[http://www.aerospaceweb.org/design/ucav/]

[35] V. Schmitt and F. Charpin. Pressure distribution on the ONERA M6 Wing at Transonic Mach numbers. AGARD AR 138 report, Office national D'etude et de recherches aerospatiales, Chatillon France. May 1979.

[36] N. Srinivas and K.Deb. Multiobjective Optimization Using Nondominated Sorting in Genetic Algorithms. Journal of Evolutionary Computation, Vol 2, No. 3, Pages 221-248.

[37] A.H.F Dias and A.Vasconcelos. Multiobjective Genetic Algorithms Applied to Solve Optimization Problems. IEEE TRANSACTIONS OF MAGNETIC, Vol. 38, No.2, Mach. 2002.

[38] J.B.Kollat and P.M.Reed. The Value of Online Adaptive Search: A Performance Comparison of NSGAII, εNSGAII and εMOEA. EMO 2005, LNCS 3410, pp. 386-398, 2005.

[39] M.Sefrioui and J.Periaux. Nash Genetic Algorithms: examples and applications. Evolutionary Computation, 2000. Proceedings of the 2000 Congress on**.** Vol.1, pp. 509-516, 2000.

[40] J.F.Wang and J.Periaux. Multi-Point Optimization using GAs and Nash/Stackelberg Games for High-Lift Multi-airfoil Design in Aerodynamics. Proceedings of the 2001 Congress on Evolutionary Computation CEC2001. pp. 552-559, 2001.

[41] D.S.Lee, L.F.Gonzalez, K.Srinivas and J.Periaux. Multi-objective Robust Design Optimisation using Hierarchical Asynchronous Parallel Asynchronous Evolutionary Algorithms, 45th AIAA Aerospace Sciences Meeting and Exhibit, Grand Sierra Resort Hotel (Formerly Reno Hilton)Reno, Nevada 8 - 11 Jan 2007.

[42] D.S.Lee, L.F.Gonzalez, K.Srinivas, D.J.Auld and J.Periaux. Multi-objective / MultiDisciplinary Design Optimisation of Blended Wing Body UAV via Advanced Evolutionary Algorithms, 45th AIAA Aerospace Sciences Meeting and Exhibit, Grand Sierra Resort Hotel (Formerly Reno Hilton)Reno, Nevada 8 - 11 Jan 2007.

Author Biographies

Dongseop Lee PhD candidate, School of AMME, University of Sydney, NSW 2006, Australia.
Birth place/date: Korea, 26.Jan.1976.
Education Background: BE (Aeronautical engineering: hons) 2004,
Major field of study: computational fluid dynamics, multiobjective and multidisciplinary design and optimisation, aircraft design.

Luis Felipe Gonzalez Lecturer, School of AMME, University of Sydney, NSW 2006, Australia.
Birth place/date: Colombia, 2.Jan.1974.
Education Background: BE 2002, PhD (aeronautical engineering) 2006.
Major field of study: computational fluid dynamics, multiobjective and multidisciplinary design and optimisation, aircraft design.

Karkenahalli Srinivas Professor, Institute of Fluid Sciences, Tohoku University 2-1-1 Katahira, Aoba-ku, Sendai 980-8577, JAPAN Ph:81 22 217 5270. Senior Lecturer, School of AMME, University of Sydney, NSW 2006, Australia.
Birth place/date: India, 18.Nov.1946.
Education Background: BE 1968, ME 1970, PhD (Mechanical Engineering) 1976.
Major field of study: computational fluid dynamics, finite volume fluid flow analysis, optimisation, MDO.

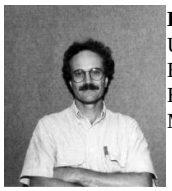

Douglass Auld Senior Lecturer, School of AMME, University of Sydney, NSW 2006, Australia.
Birth place/date:
Education Background: BSc, BE, MEngSc, PhD.
Major field of study: aerospace engineering, DSMC.

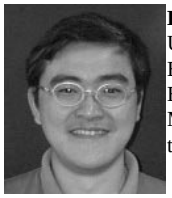

Kee Choon Wong Senior Lecturer, School of AMME, University of Sydney, NSW 2006, Australia.
Birth place/date:
Education Background: BE, PhD.
Major field of study: aircraft design, aircraft construction techniques, UAV.